

R. Yamazaki¹, N. Ishizaka¹, S. Kakuchi¹, S. Sei¹, K. Sugiyama¹, K. Aihara¹,
S. Kanbayashi¹, S. Tomita^{1,7}, S.J. Tanaka¹, Y. Sakawa², T. Sano², M. Ota²,
S. Egashira², T. Izumi², R. Kumar², Y. Kuramitsu², K. Tomita³, T. Morita³,
M. Edamoto³, S. Matsukiyo³, H. Yoneda⁴, N. Ohnishi⁵, T. Umeda⁶, Y. Ohira⁷,
A. Ishii⁸, and T. Takezaki⁹

¹ Aoyama Gakuin University, ² Osaka University, ³ Kyushu University,

⁴ University of Electro-communications, ⁵ Tohoku University, ⁶ Nagoya University,

⁷ University of Tokyo, ⁸ Max Planck Institute for Gravitational Physics (Potsdam),

⁹ National Institute of Technology, Kitakyushu College



実験室宇宙物理学

- ・(現場にいくのが不可能な)宇宙空間で起こる現象・物理過程を地球上で再現する。
=> 宇宙空間で起こる現象とは対照的に
 - ・制御可能: 好きな状況を作れる。
 - ・「その場」観測により豊富なデータが得られる。

実験室宇宙物理の発展により

- ・未解明の現象・物理過程を理解できるかもしれない。
- ・新たな天体现象を予言できるかもしれない。
- ・予想もしなかった物理現象の発見につながるかもしれない。

天文観測、理論計算・シミュレーションに続く第3の独立な研究ツールとしたい！

実験室宇宙物理学

今回は大型レーザーを用いた衝撃波実験の紹介がメインだが、

実験室宇宙物理はレーザー実験が全てではない。

例: MRI, SASI, Shocks...

大型レーザー(NIF, OMEGA,...)を使った実験の例:

EOS測定,

リコネクション,

リヒトマイヤー・メシュコフ不安定

jet伝播,

磁気乱流(ダイナモ, 乱流中の粒子拡散),

プラズマ不安定(current instabilities, Bell instability,...)

“レーザー”宇宙物理学

大型レーザーを用いた無衝突衝撃波やリコネクション実験：

vs. PIC simulations:

PICでは計算できない長時間スケール、大空間スケールまで実験可能。

「PIC計算では〇〇〇が見えている。」というのと同様に、すでに(少なくとも密度・温度・磁場等の物理量については)
「レーザー実験では〇〇〇が見えている。」と言えるところまできた。

Experimental parameters

Parameters of unshocked plasma:

$$n_e \sim n_i \sim 10^{18} \text{ cm}^{-3}, \quad T_e \sim T_i \sim 100 \text{ eV}, \quad B \sim 1 \text{ T}$$

$$\Rightarrow \text{plasma parameter: } n_e \lambda_{De}^3 \sim 4 \times 10^2 (\propto n^{-1/2} T^{3/2})$$

$$\text{electron skin depth: } c/\omega_{pe} \sim 10^{-3} \text{ mm } (\propto n^{-1/2})$$

$$\text{plasma beta: } \beta \sim 40 (\propto n T B^{-2})$$

$$\text{freq. ratio: } \omega_{pe}/\omega_{ce} \sim 3 \times 10^2 (\propto n^{1/2} B^{-1})$$

$$\text{Alfven velocity: } v_A \sim 2 \times 10^6 \text{ cm/s } (\propto n^{-1/2} B)$$

$$\text{sound velocity: } c_s \sim 10^7 \text{ cm/s } (\propto T_i^{1/2})$$

$$\text{gyro radius of thermal } e\text{'s: } r_{g,e} \sim 10^{-2} \text{ mm } (\propto T_e^{1/2} B^{-1})$$

$$\text{gyro radius of thermal ions: } r_{g,i} \sim 1 \text{ mm } (\propto T_i^{1/2} B^{-1})$$

$$\Rightarrow \text{For } M_s \sim 10 \quad (v_s \sim 10^8 \text{ cm/s}, M_A \sim 50),$$

$$\text{downstream temp.(simply by RH): } T_d \sim 32 \quad T_u \sim 3 \text{ keV}$$

$$\Rightarrow \text{required system size} > 1 \text{ cm. or } B \gg 1 \text{ T ?}$$

Ion mean free path for Coulomb collision:

$$\lambda_{ii} = \frac{m_p^2 v_{sh}^2}{8\pi n_0 Z^4 e^4 \ln \Lambda} = 7.0 \times 10^{18} \text{ cm} \frac{v_8^4}{Z^4 n_0} \left(\frac{\ln \Lambda}{30} \right)^{-1}$$

$$\ln \Lambda = \ln \left[\frac{m_p v_{sh}^2}{Z^2 e^2} \sqrt{\frac{k T_0}{4\pi n_0 e^2}} \right] = 32 + \ln \left[(v_8/Z)^2 \sqrt{T_{eV}/n_0} \right]$$

レーザープラズマの業界の「collisionless (shock)」の定義：

この λ_{ii} が system size (または衝撃波遷移層)よりも大きいとき collisionless。

レーザープラズマの人たちのプレゼンを聞くときは、
宇宙物理・天体物理の業界の定義とは異なることに注意が必要。

銀河団、超新星残骸、太陽風、実験室の衝撃波で、 マツハ数と特徴的長さの大小関係はどれも同じ：

	n_0 (cm $^{-3}$)	T_0 (K)	v_{sh} (cm s $^{-1}$)	B_0 (μG)	L_{sys} (cm)	Δ_{obs} (cm)	λ_{ii} (cm)	$r_{g,i}$ (cm)	L_i (cm)	ω_{pe}/ω_{ce}	β	M_A	M_s	M_{el}
Clusters	10^{-3}	10^8	10^8	1	10^{25}	10^{22}	10^{22}	10^{10}	10^9	10^2	10^2	10	1	10^{-2}
SNRs	1	10^4	10^8	10	10^{19}	10^{16}	10^{19}	10^9	10^7	10^2	1	10^3	10^2	1
SW (TS)	10^{-3}	10^5	10^8	0.1	10^{15}	10^9	10^{22}	10^{10}	10^9	10^2	1	10	10	1
SW (1 AU)	10	10^5	10^8	10	10^{12}	10^6	10^{19}	10^9	10^7	10^2	1	10^2	10	1
Laboratories	10^{17}	10^5	10^8	$< 10^{10}$	1	10^{-3}	10^2	> 1	10^{-1}	$> 10^2$	< 1	10	10	1

$$M_{el} < M_s \leq M_A$$

$$L_i < r_{g,i} \ll \lambda_{ii}$$

ついでに どの場合も、プラズマ $\beta \sim O(1)$.

M_{el} : electronic sonic Mach number,

L_i : ion skin depth,

M_s : sonic Mach Number,

$r_{g,i}$: ion gyro radius,

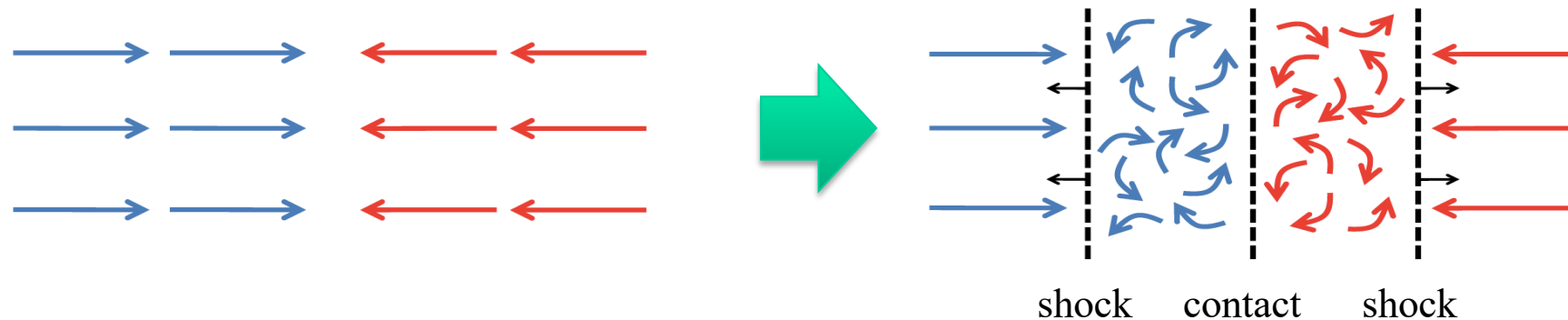
M_A : Alfvén Mach number,

λ_{ii} : ion Coulomb m.f.p.

Collisionless shocks are ubiquitous

Shocks

- * are ubiquitous in various astrophysical, heliospheric, and laboratory plasmas.
 - examples will be shown later !
- * arise when two counter-streaming supersonic flows interact.



- * are, in most cases, “collisionless” mainly because of low-density:
 - Coulomb mean-free-path is much larger than the system size.
 - Particle distribution NOT going to perfect Maxwellian.
 - Various components arise during dissipation process.
- * consist of multi-scale physics:
 - electron/ion kinetic scales (\ll size of objects) are important for dissipation.
 - all scales are nonlinearly coupled (e.g., Umeda, RY+11)

Unsolved problems on shock physics

- * Dissipation mechanism of the collisionless shocks:

- gas heating mechanism ? (T_e , T_i just downstream ?)
- energy partition among various components (e, i, B, rela, waves, turb,...) ?

- * Shock structure:

- electron scale waves?
- ion scale: ripples, shock reformation?
- back reactions of accelerated particles (\Rightarrow shock modification) ?

- * Injection to Fermi acceleration process:

- particle acceleration is one of dissipation mechanisms !
- injection rate?

All these processes may be coupled !

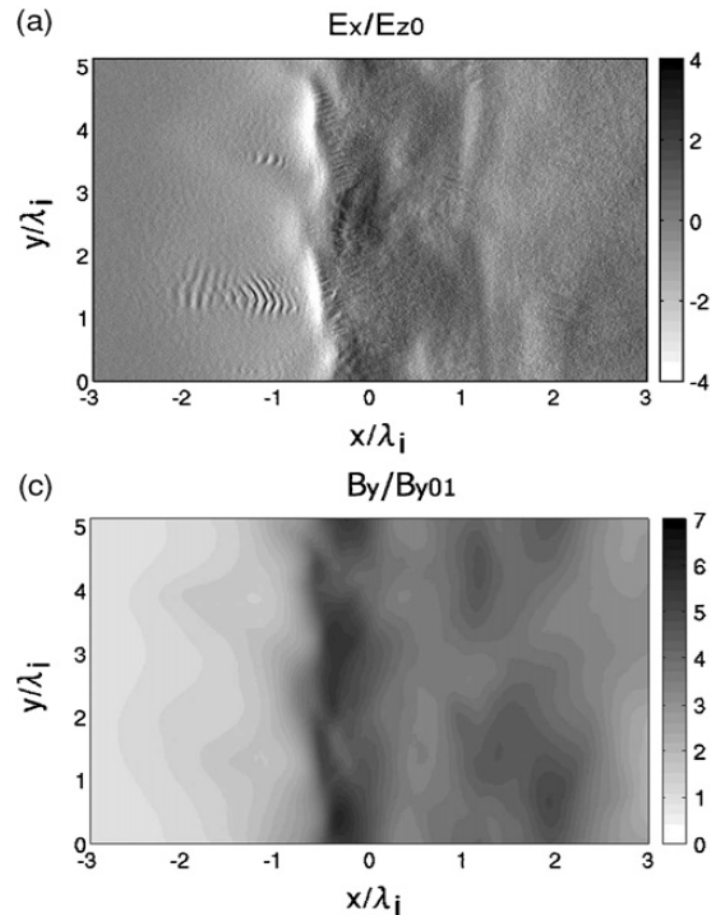
How do the above processes depend on upstream conditions ?

- Mach numbers (M_A , M_s , M_{el})
- plasma β
- shock angle
- ionization fraction

PIC simulation for low- M shocks

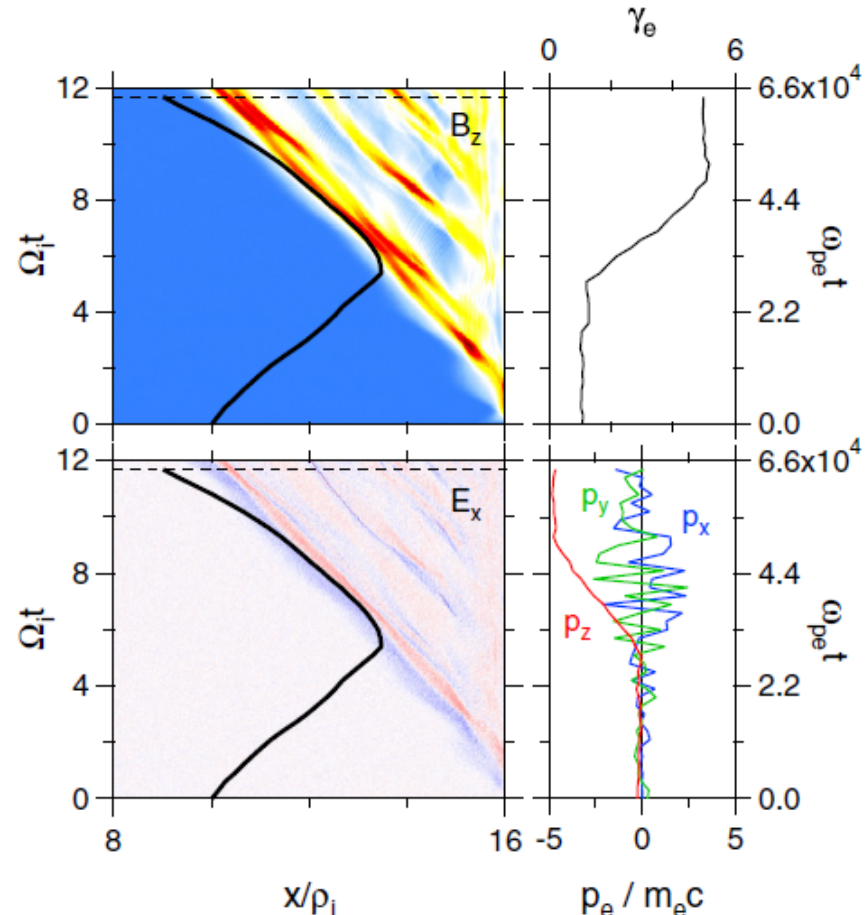
Our simulation studies on electron acceleration.

Umeda, RY+ (2009)



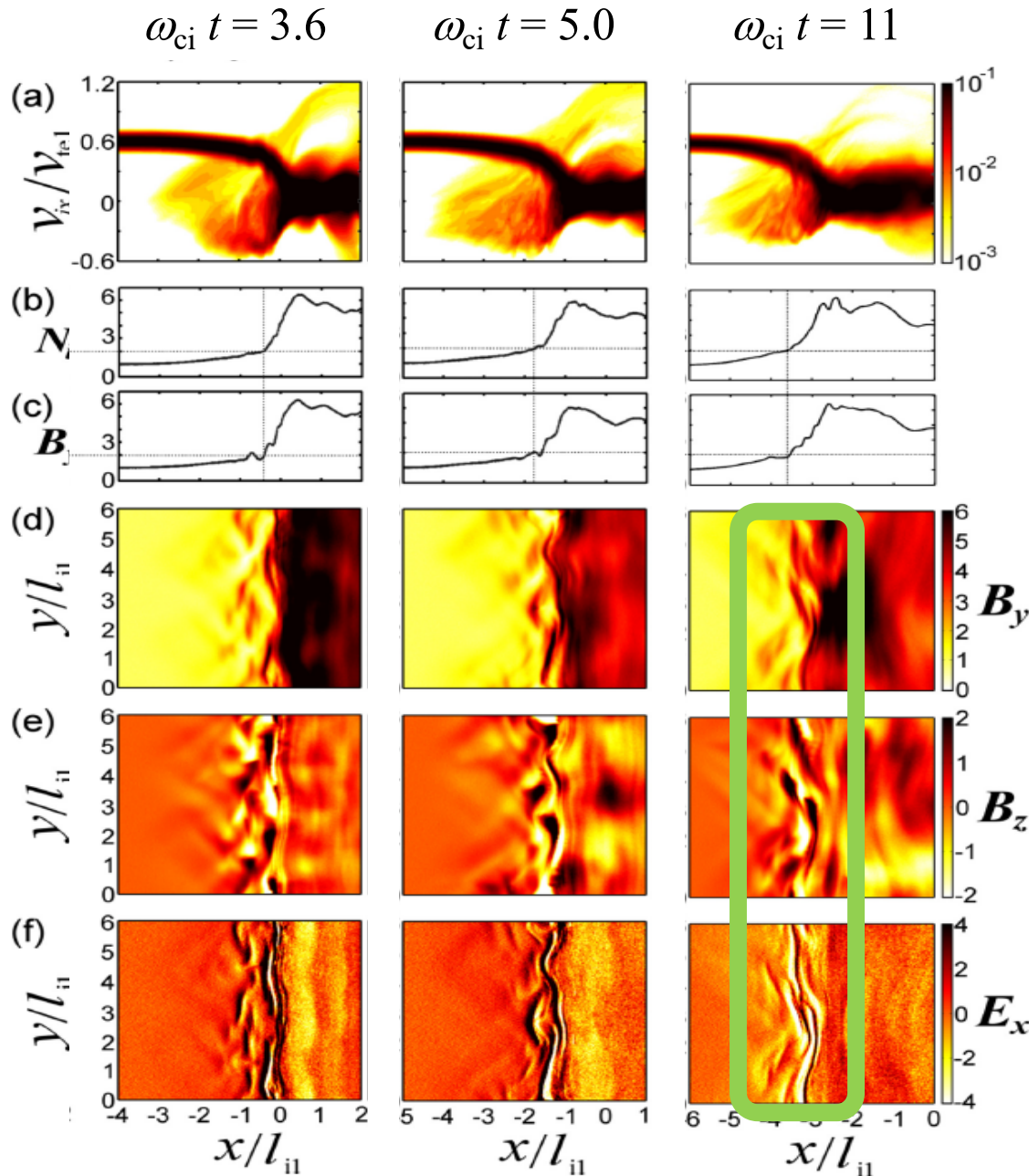
Surfing acceleration by ESW emitted by shock ripple.

Matsukiyo, Umeda, RY + (2012)



Shock drift acceleration in high-beta case, seen in cluster shocks.

PIC simulation for low- M shocks



Umeda, RY + 12, 14:
2D PIC simulations of perp. shocks

- in-plane, perp. B-field
- upstream parameters:
 $\beta = 0.32, M_A \sim 6$

イオン温度非等方不安定
 ⇒ 電磁イオンサイクロトロン波
 ⇒ Ripple

Umeda, RY+12, 14

PIC simulation for low- M shocks

Yamazaki +2019 :

2D PIC simulations, Run D: $M_A = 4.6$, $\beta = 0.08$

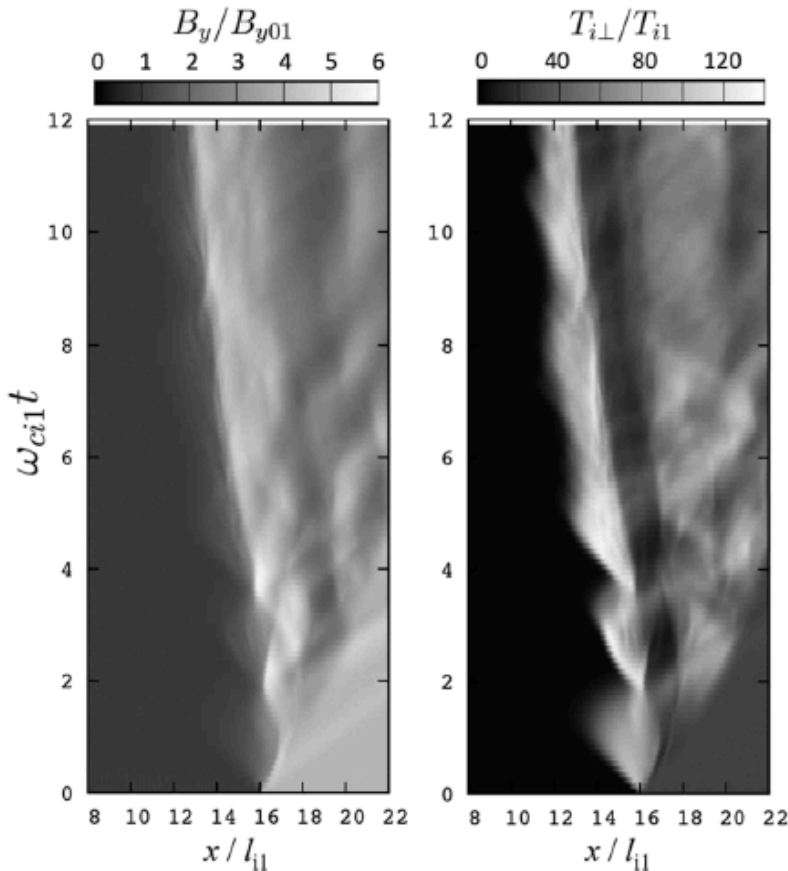


FIG. 1. Spatiotemporal diagram of the y -component of magnetic field B_y and ion perpendicular temperature $T_{i\perp}$ for Run D. Both B_y and $T_{i\perp}$ are averaged over the y direction. Initial unphysical discontinuity is located at $x = 16l_{i1}$.

Footで $T_{i\perp}$ 最大。
Overshootで $T_{i\perp}$ 極小。

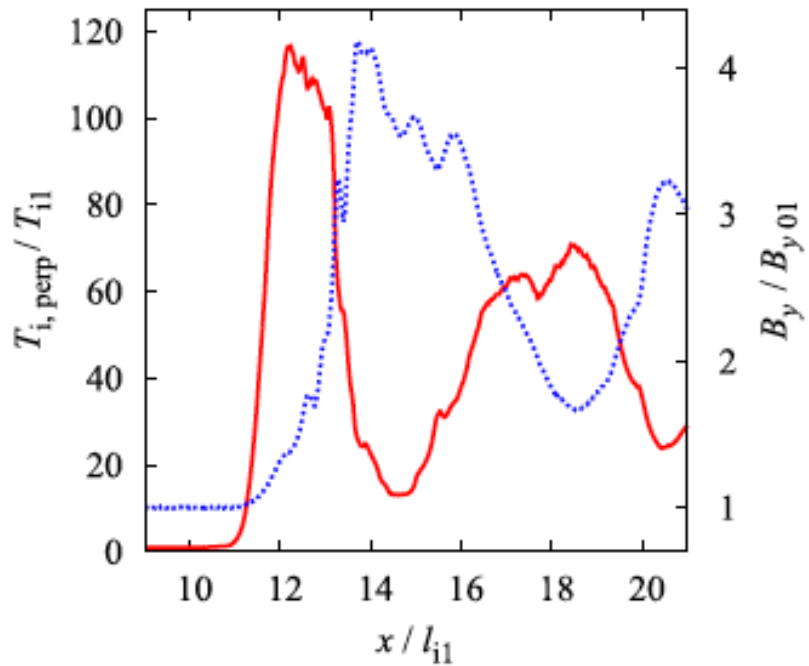


FIG. 2. Spatial profile of ion perpendicular temperature averaged over the y direction $T_{i\perp}$ (thick solid curve) and the y -component of the magnetic field averaged over the y direction B_y (dotted curve) at $\omega_{ci}t = 9.96$ of Run D.

PIC simulation for low- M shocks

Yamazaki +2019 : 2D PIC simulations, 6 runs

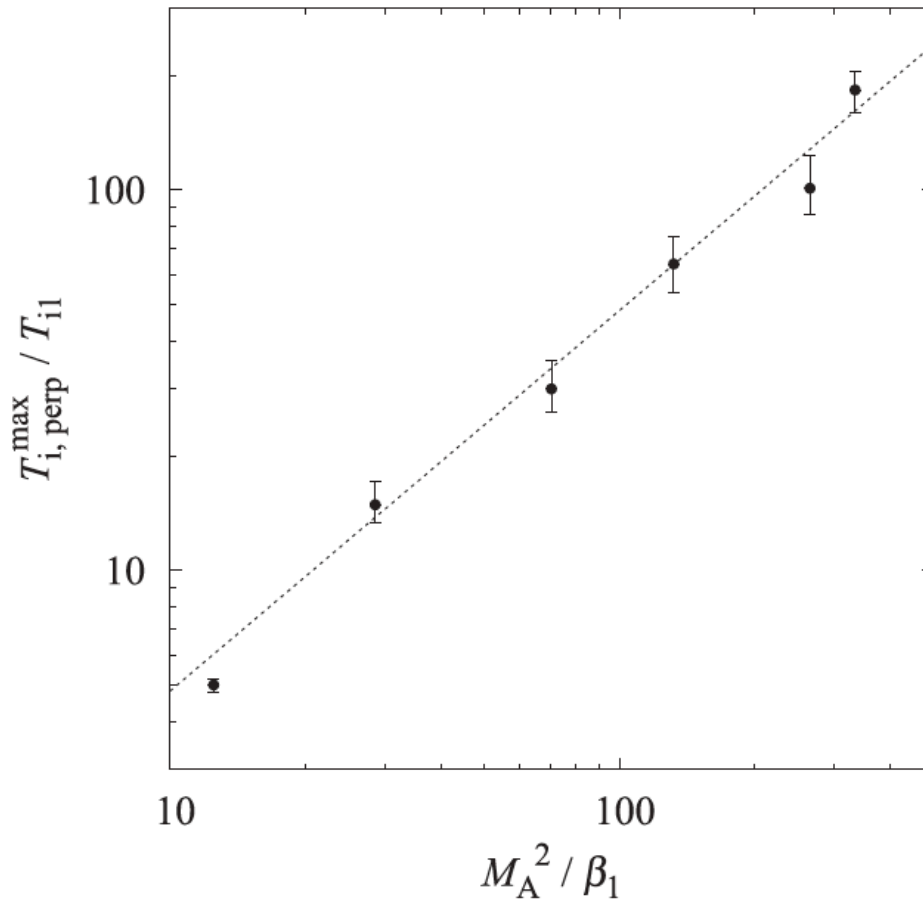


FIG. 3. Ion perpendicular temperature $T_{i\perp}^{\max}$ as a function of M_A^2/β_1 . Triangles represent $\langle T_{i\perp}^{\max} \rangle / T_{i1}$, while error bars indicate the maximum and minimum values of $T_{i\perp}^{\max} / T_{i1}$, which are given in Table I. All the values are obtained for $7 < \omega_{ci}t < 12$. The dotted line represents best-fitted linear relation, $T_{i\perp}^{\max} / T_{i1} = 0.48 \times M_A^2 / \beta_1$.

Studies of collisionless shocks

Methods	Pros	Cons
Observations of astrophysical objects	<ul style="list-style-type: none">▪ see the whole system.▪ see evolved ($t \rightarrow \infty$).▪ less boundary effects.	<ul style="list-style-type: none">▪ difficult to see time evolution.▪ worse angular resolution.▪ unable to directly measure distribution functions, elemag fields.
“In-situ” observations by satellites	<ul style="list-style-type: none">▪ rich observables (distribution func./elemag fields).▪ short cadence	<ul style="list-style-type: none">▪ $M \sim 10$: uncontrollable.▪ only measurable at satellites.
Simulations	<ul style="list-style-type: none">▪ set initial and boundary conditions.▪ see all observables at arbitrary place and epoch.	<ul style="list-style-type: none">▪ huge CPU time in 3D cases▪ unrealistic parameters.▪ limited spatial and time scales
Laboratory Experiments	<ul style="list-style-type: none">▪ set initial and boundary conditions.▪ see all observables at arbitrary place and epoch.▪ Real parameters/physical quantities.	<ul style="list-style-type: none">▪ less people joining!▪ limited spatial and times scales.▪ methods unestablished.

Previous shock experiments

- Many collisional shock generation (many authors)
- Collisionless shocks in unmagnetized plasmas: w/o external B.
 - Kuramitsu et al. (2011) with GXII: electrostatic shocks.
 - Sakawa et al. (2019) with NIF: “Weibel” shocks.
- Collisionless shocks in magnetized plasmas: w/ external B.
 - Paul et al. (1965) via Z-pinch: $M_A < 10$
 - Niemann et al. (2014) with UCLA/LAPD: $M_A < 2$
 - Schaeffer et al. (2017, 2019) with OMEGA: $M_A > \sim 10$

Our advantage over previous works:

- * simultaneous measurements of density and temperature across the shock via *collective Thomson scattering*, as well as B-field.
- * simple setup to have supercritical magnetized shock: $M_A > 3$

Previous shock experiments

- Many collisional shock generation (many authors)
- Collisionless shocks in unmagnetized plasmas: w/o external B.
 - Kuramitsu et al. (2011) with GXII: electrostatic shocks.
 - Sakawa et al. (coming soon?) with NIF: “Weibel” shocks.

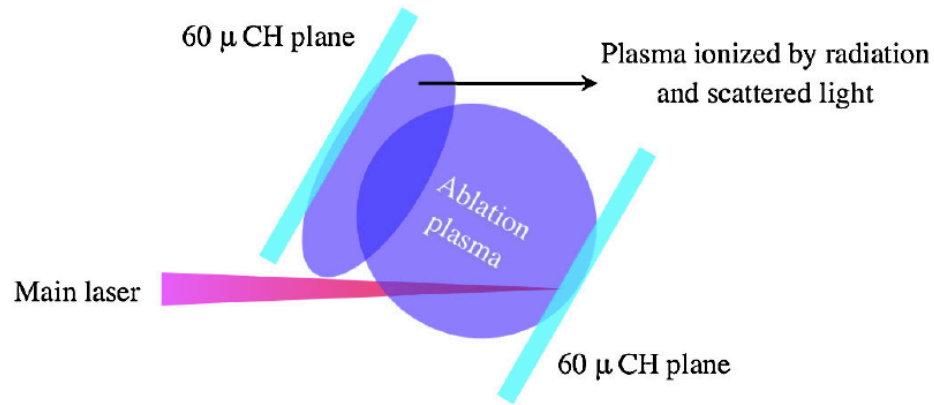
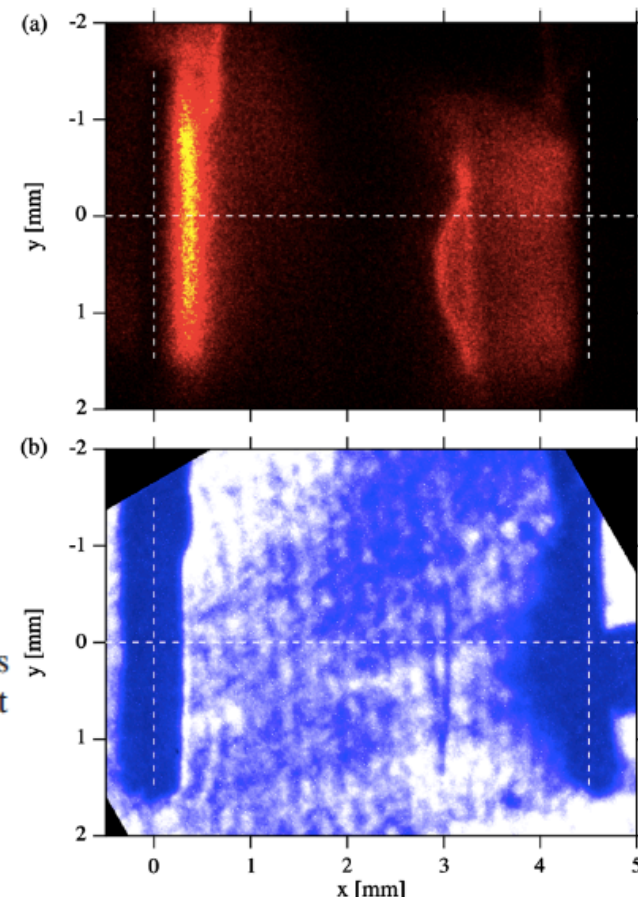


FIG. 1 (color online). Schematic of the double-plane target. The separation between two planes was 4.5 mm. The target normal lies 30° from the laser axis.

FIG. 4 (color online). (a) Self-emission snapshot at $t = 25$ ns taken on the same shot as Fig. 2. (b) Shadowgraphy snapshot at $t = 25$ ns taken on a different shot.

Kuramitsu et al. (2011), PRL



Previous shock experiments

- Collisionless shocks in magnetized plasmas: w/ external B.
 - Paul et al. (1965) via Z-pinch: $M_A < 10$.
 - Morita et al. (2013) with GekkoXII: $M_A \sim 1$.
 - Niemann et al. (2014) with UCLA/LAPD: $M_A < 2$.
 - Schaeffer et al. (2017) with OMEGA: $M_{ms} \sim 12$.

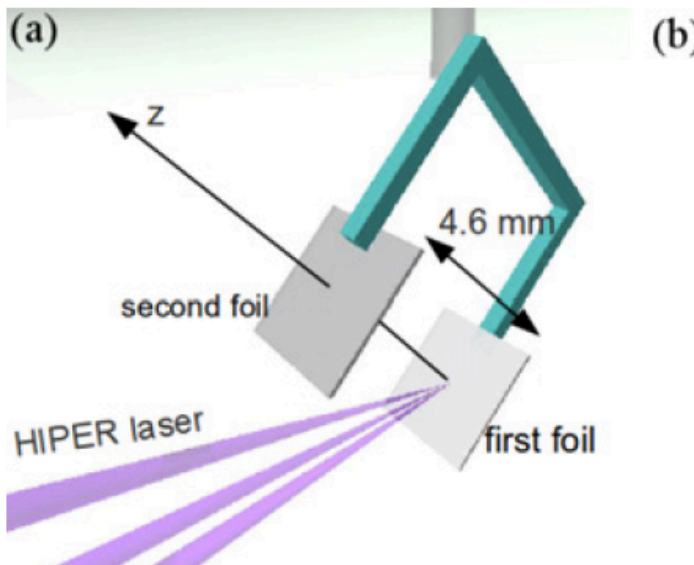
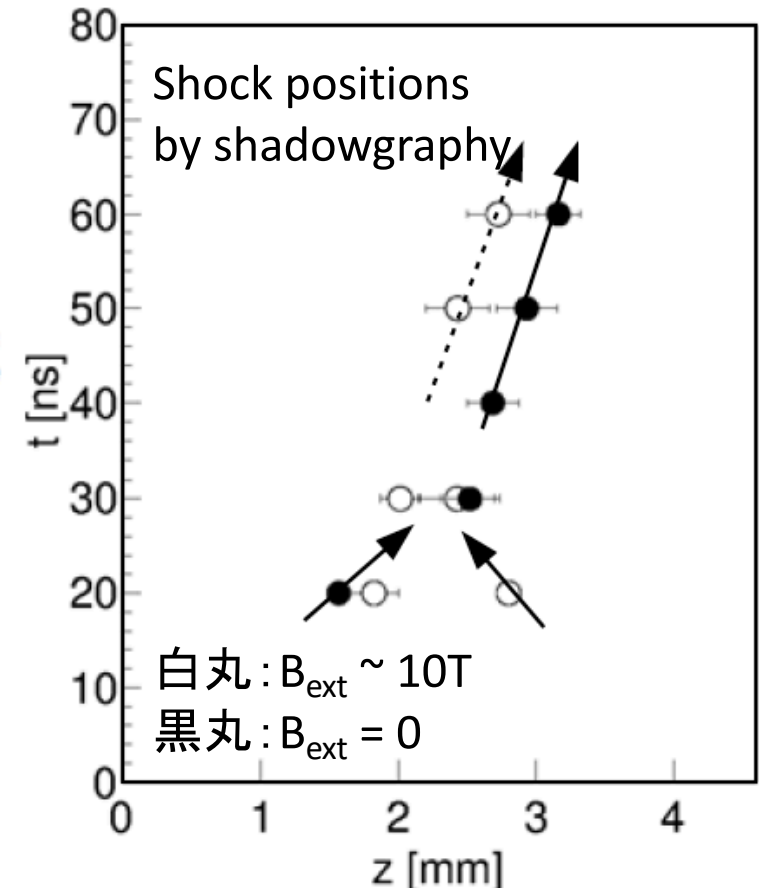


Figure 1. (a) The schematic view of the target. The first foil is irradiated by three beams to produce counter-streaming plasmas between two foils. (b) The top view of the target. The plasmas are diagnosed by the SG, GOI, SI, and SOP from the direction perpendicular to the plasma expansion.



Previous shock experiments

- Collisionless shocks in magnetized plasmas: w/ external B.
 - Paul et al. (1965) via Z-pinch: $M_A < 10$.
 - Morita et al. (2013) with GekkoXII: $M_A \sim 1$.
 - Niemann et al. (2014) with UCLA/LAPD: $M_A < 2$.
 - Schaeffer et al. (2017) with OMEGA: $M_{ms} \sim 12$.

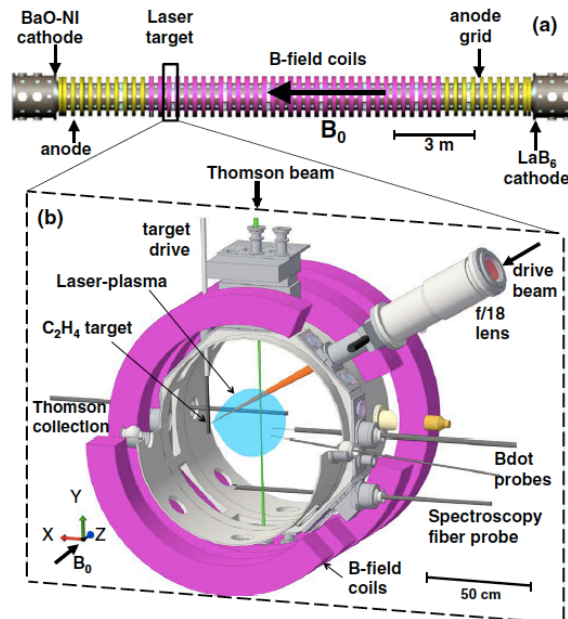
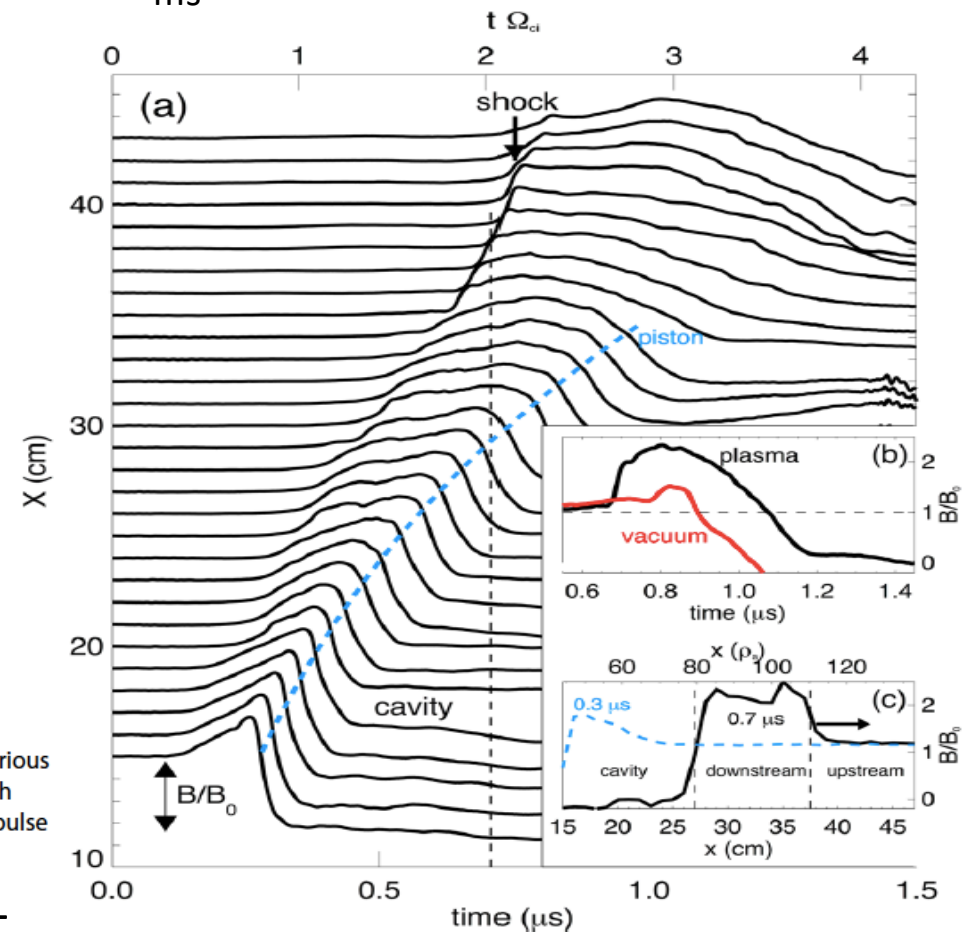


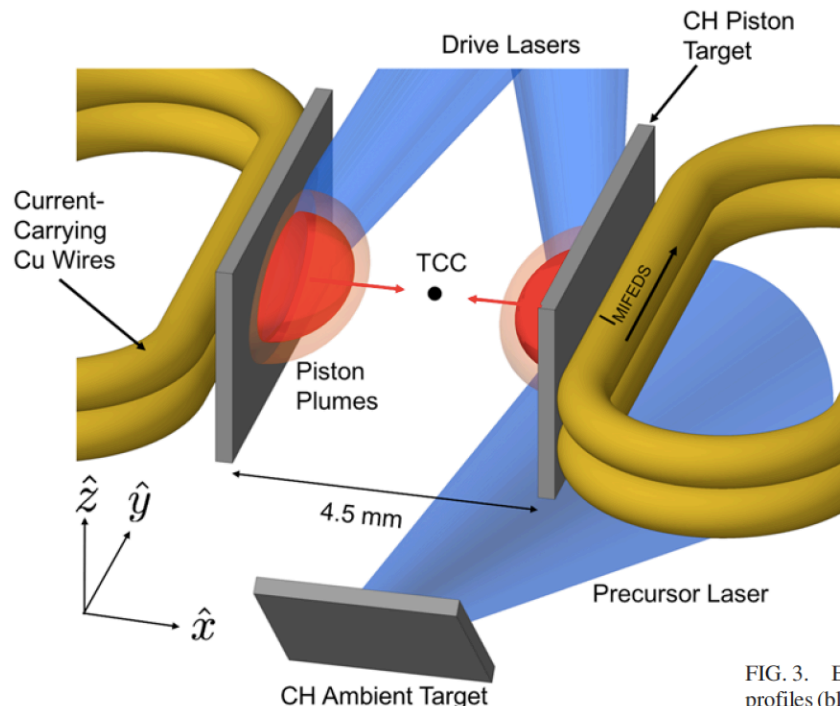
Figure 1. Schematic of (a) the LAPD and (b) the laser-target and diagnostics configuration.

Figure 2. (a) Magnetic stack plots of B_z as a function of time for various distances from the target. (b) Comparison of $B_z(t)$ at $x = 35$ cm with (black) and without (red) the ambient plasma. (c) Structure of the pulse before ($t = 0.3$ μ s) and after a shock is formed ($t = 0.7$ μ s).



Previous shock experiments

- Collisionless shocks in magnetized plasmas: w/ external B.
 - Paul et al. (1965) via Z-pinch: $M_A < 10$.
 - Morita et al. (2013) with GekkoXII: $M_A \sim 1$.
 - Niemann et al. (2014) with UCLA/LAPD: $M_A < 2$.
 - Schaeffer et al. (2017) with OMEGA: $M_{ms} \sim 12$.



Schaeffer et al. (2017), PRL

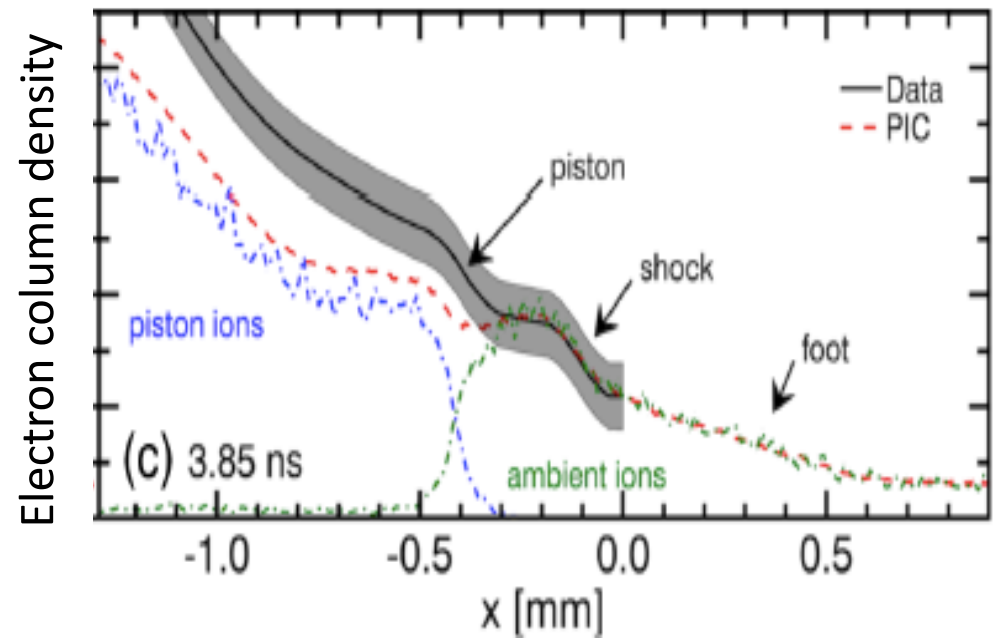
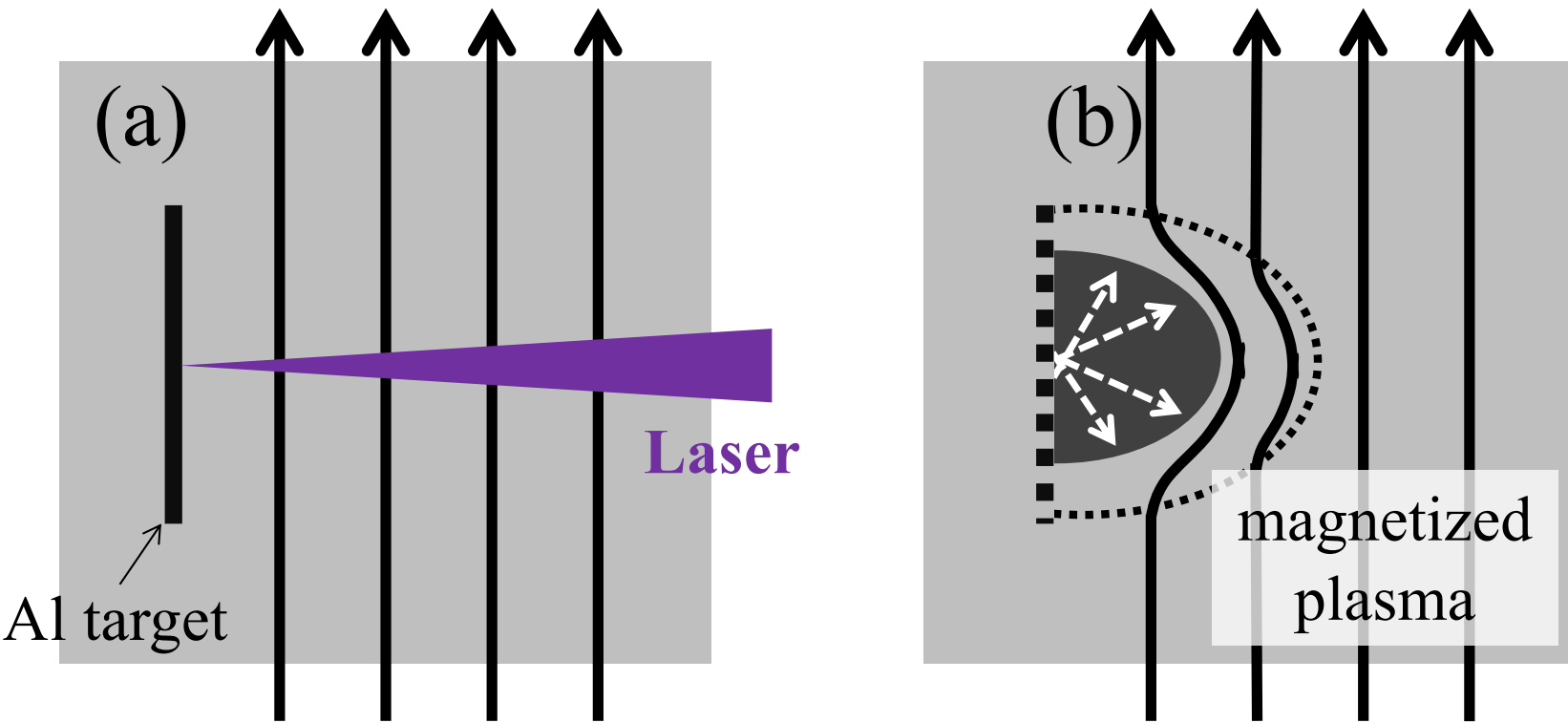


FIG. 3. Evolution of line-integrated electron density profiles at (a) 2.35, (b) 2.85, and (c) 3.85 ns after laser ablation. For each, the density profiles (black) were reconstructed by linearly interpolating between the gradient density values associated with each AFR band edge and, in the regions of the density jumps, utilizing the shadowgraphy profiles. The constant density offset was estimated from simulations, and the shaded band corresponds to the uncertainty in this offset. Also shown are the corresponding profiles from PSC PIC simulations (red). Additionally, in (c) the ambient (green) and piston (blue) contributions to the total electron density in the PIC simulations are shown. [(a), inset] Raw shadowgraphy signal (black) and reconstructed relative density (green) profile at 2.35 ns. [(b), inset] Direct comparison of the raw AFR signal (black) and corresponding synthetic simulation signal (red) at 2.85 ns. For both, the signals have been reduced to binary for simplicity. In all plots, the plasma moves toward $x = 0$.

Experimental setup



- (a) Magnetic field (solid arrows) is supplied around a plane target, and the target is irradiated by high-energy laser.
- (b) The target ejects plasma and ionizing photons. Gas is ionized and simultaneously magnetized. Target plasma pushes magnetized plasma (white arrows) to generate a collisionless shock (dotted curve).

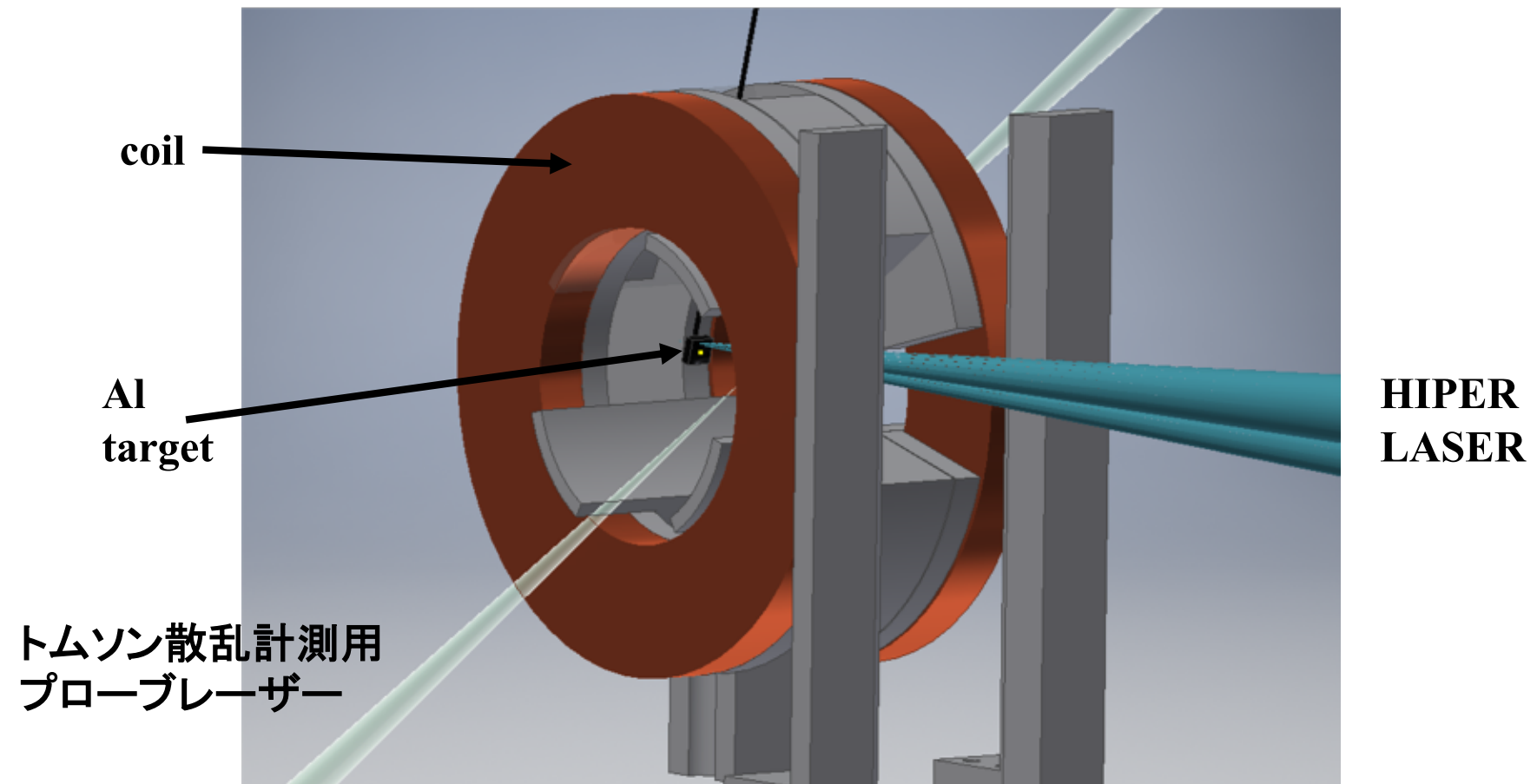
External magnetic field

- Edamoto et al. 2018, Rev. Sci. Instr.

Coils: inner diam.= 60 mm, outer diamm.=110 mm (separation = 25mm)

Capacitors: $3000\mu\text{F} \times 4$ (max vol. =1.4 kV) ($\Rightarrow I \sim 4000 \text{ A}$)

Imposed B-field: $\sim 3.6 \text{ T}$, duration $\sim 100 \mu\text{s}$.



外部磁場印加装置

3年間にわたり 3D CAD で設計

- 中性ガス中の放電

V_{min} [v] : 放電電圧

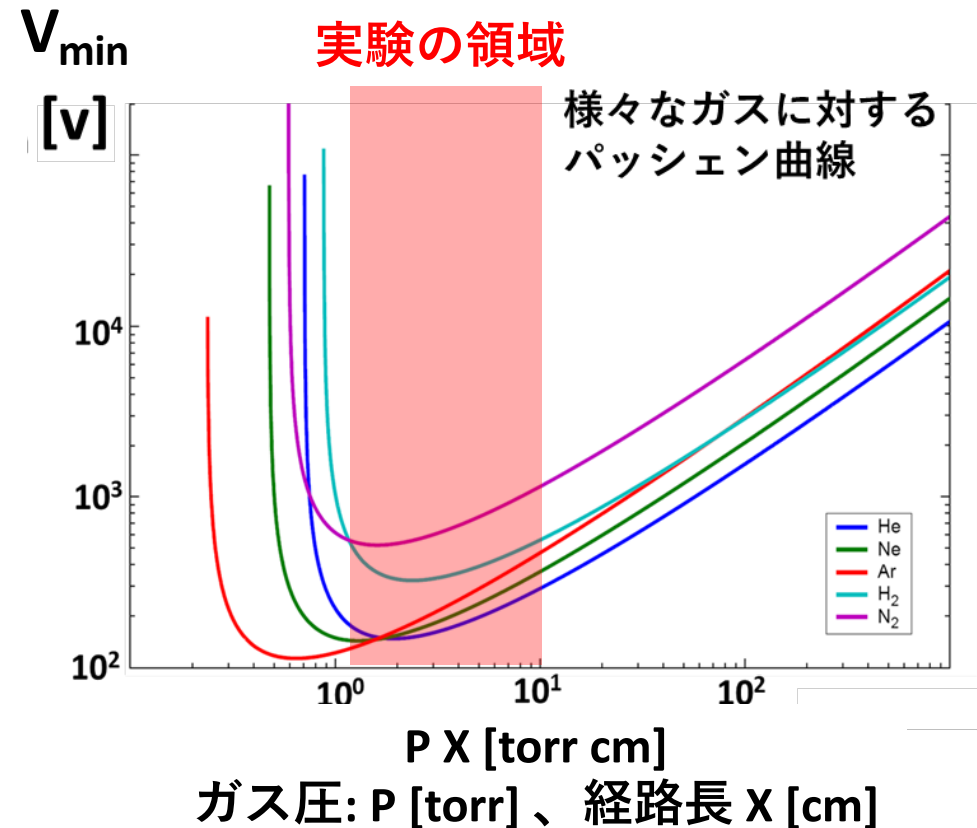
これ以上の電圧では放電が起こる

高磁場のために高電圧を
かけたいが放電する

- 空間的な配置の難しさ

ターゲット導入、ハイパーレーザー、計測用レーザーを避けて
装置を配置する必要がある

数 μm 精度の実験デザインの
設計が必要



外部磁場印加装置の開発

実験開始3年目までは外部磁場が印加できなかった。



3D CADソフトを用いた精密設計の導入により
初の外部磁場印加実験に成功。



徐々に強磁場が印加可能になってきた。

2017年度:0.5 T、 2018年度:1.6 T、 2019年度:3.6 T

2019年度の装置は1回のみ磁場を印加可能。

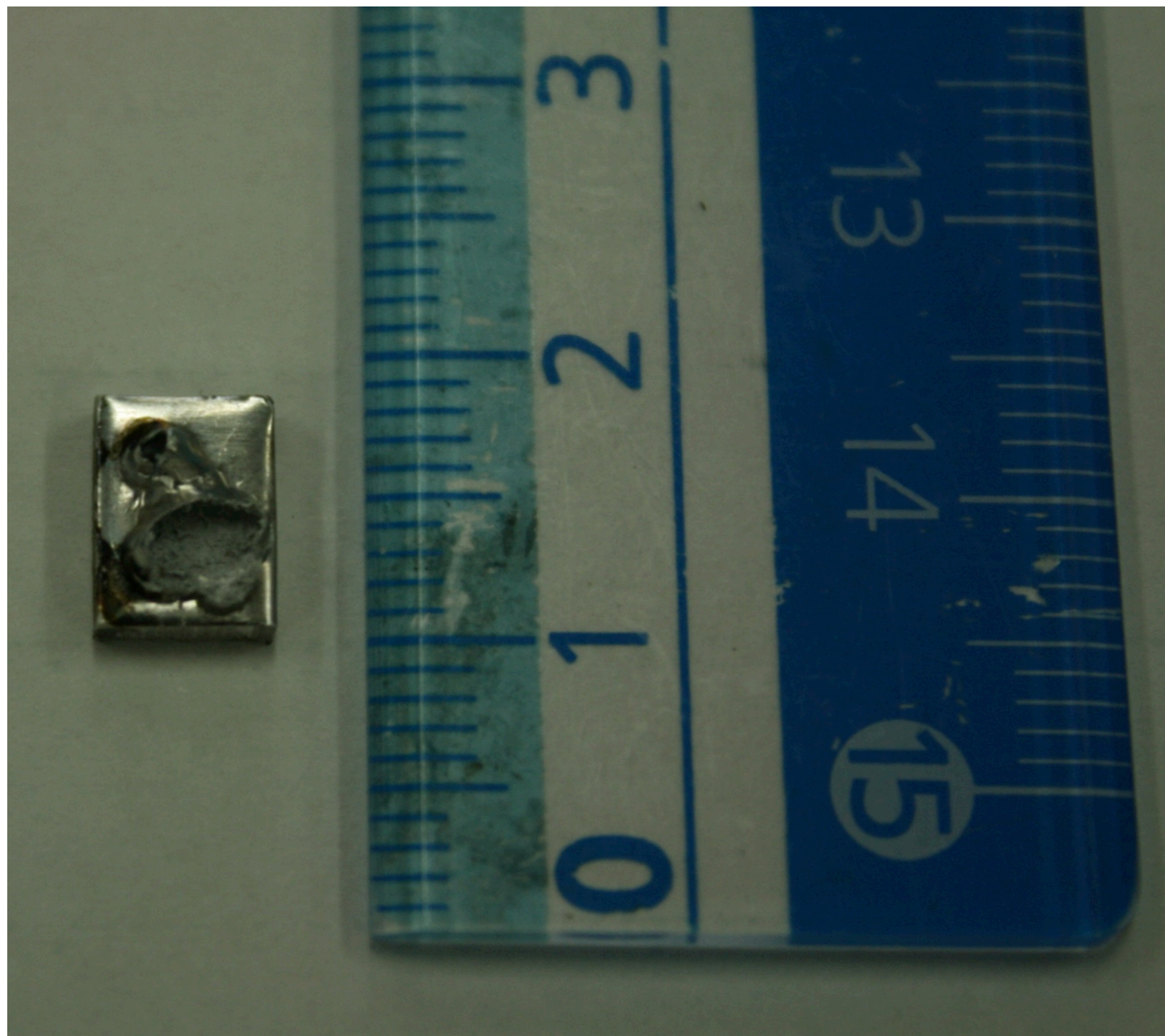


来年度は装置のストックを多数作ることで
目標としていた実験実験環境で複数回実験が可能。



実験デザインの決定

ショット後に回収したターゲット

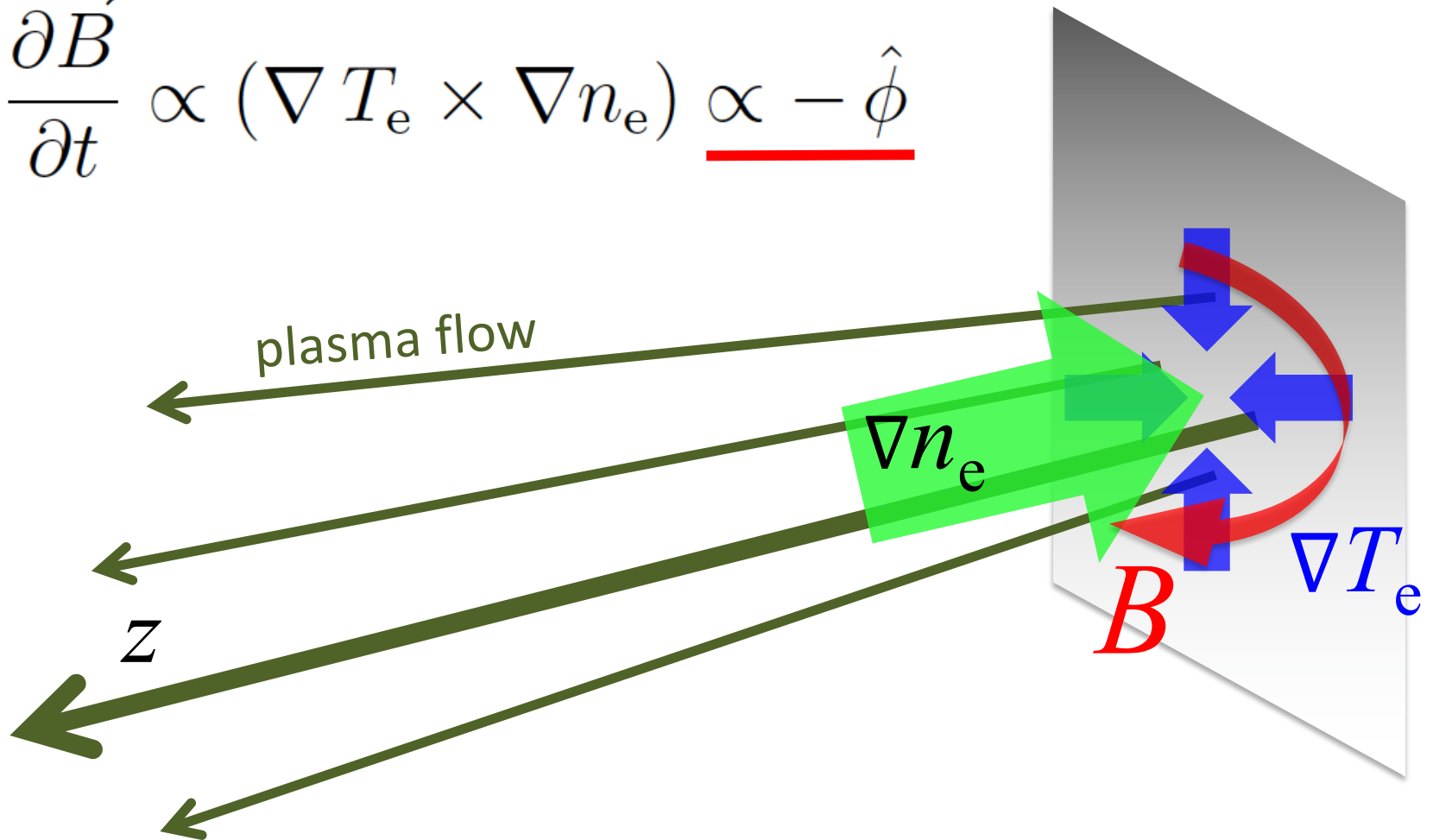


Gregori et al. 12, Nature; Kugland et al. 12, Nature Phys.:

Ablation plasma (piston plasma) is magnetized via Biermann effect.

$$\nabla T_e \propto -\hat{r} , \quad \nabla n_e \propto -\hat{z}$$

$$\rightarrow \frac{\partial \vec{B}}{\partial t} \propto (\nabla T_e \times \nabla n_e) \propto -\hat{\phi}$$



Gregori et al. 12, Nature; Kugland et al. 12, Nature Phys.:

Ablation plasma (piston plasma) is magnetized via Biermann effect.

$$\nabla T_e \propto -\hat{r} , \quad \nabla n_e \propto -\hat{z}$$

$$\rightarrow \frac{\partial \vec{B}}{\partial t} \propto (\nabla T_e \times \nabla n_e) \propto -\hat{\phi}$$

$$\begin{aligned} \rightarrow B &\approx \frac{T_e}{eV_d\phi} \\ &\sim 10 \text{ T} \left(\frac{T_e}{10^3 \text{ eV}} \right) \left(\frac{V_d}{10^2 \text{ km/s}} \right)^{-1} \left(\frac{\phi_f}{1 \text{ mm}} \right)^{-1} \end{aligned}$$

(T_e : electron temp., V_d : flow velov., ϕ_f : focal spot size)

輻射流体シミュレーション

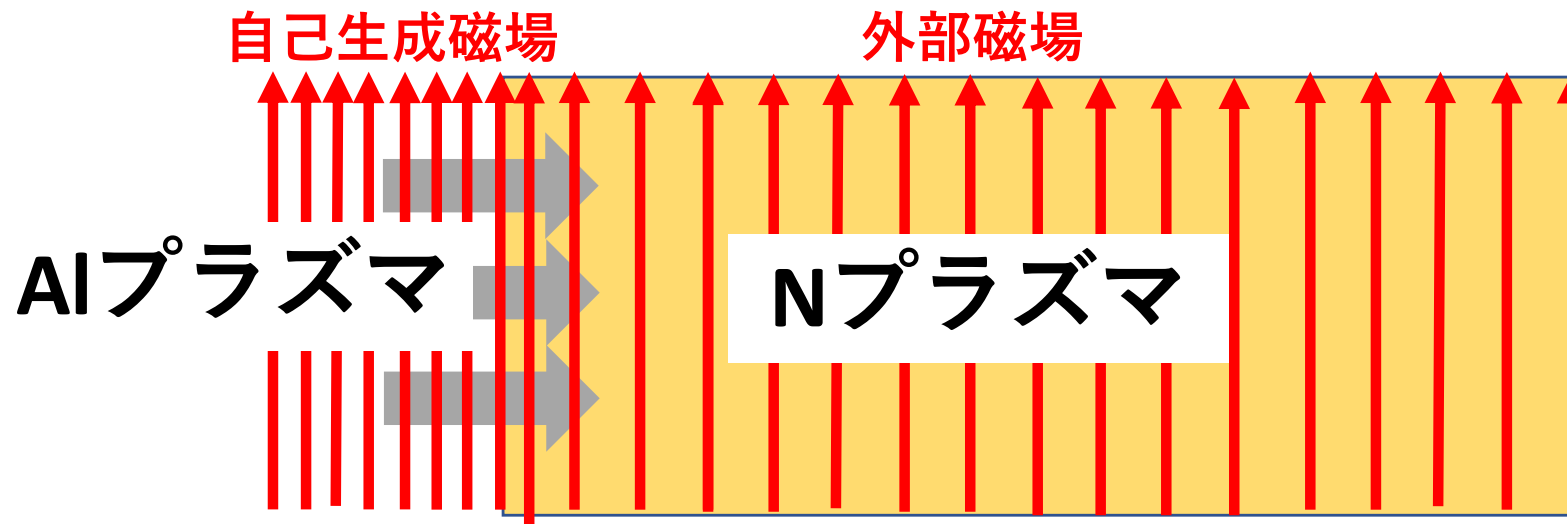
- まず輻射流体計算を行う(PheNiX:大西直文氏提供):
 軸対称2次元。
 入射レーザー: 10^{14} W/cm^2 , パルス幅1.3 ns, 波長1053 nm
 ターゲットはAl (1mm厚)。(雰囲気ガスは窒素1torr)
 → レーザー照射後の電子密度・温度の発展を求める。
- Post processでBierman 磁場を求める。

$$\frac{\partial \vec{B}}{\partial t} = \underbrace{\nabla \times (\vec{v} \times \vec{B})}_{\text{対流項}} + \underbrace{\frac{c}{n_e^2 e} (\nabla p_e \times \nabla n_e)}_{\text{Biermann 項}}$$

1D プラズマ粒子シミュレーション : Umeda et al ('19)

1D Particle In Cell (電磁粒子シミュレーション)

Maxwell 'eq と荷電粒子のEoMを同時に解く。
双方の磁場強度を色々変えてプラズマの様子の変化を調べた。



$$B_{AI} = 0 \text{ T}, 10 \text{ T}$$

$$m_i/m_e = 49572$$

$$T_e = 10 \text{ eV}$$

$$n_e = 3.75 \times 10^{19} / \text{cc}$$

$$v = 500 \text{ km/s}$$

$$B_N = 0 \text{ T}, 1.5 \text{ T}, 3 \text{ T}, 5 \text{ T}$$

$$m_i/m_e = 25704$$

$$T_e = 30 \text{ eV}$$

$$n_e = 1.5 \times 10^{18} / \text{cc}$$

$$v = 0 \text{ km/s}$$

計算コスト節約のため、以下を仮定。

光速 $C = 3.0 \times 10^9 \text{ cm/s}$ (現実の10分の1)

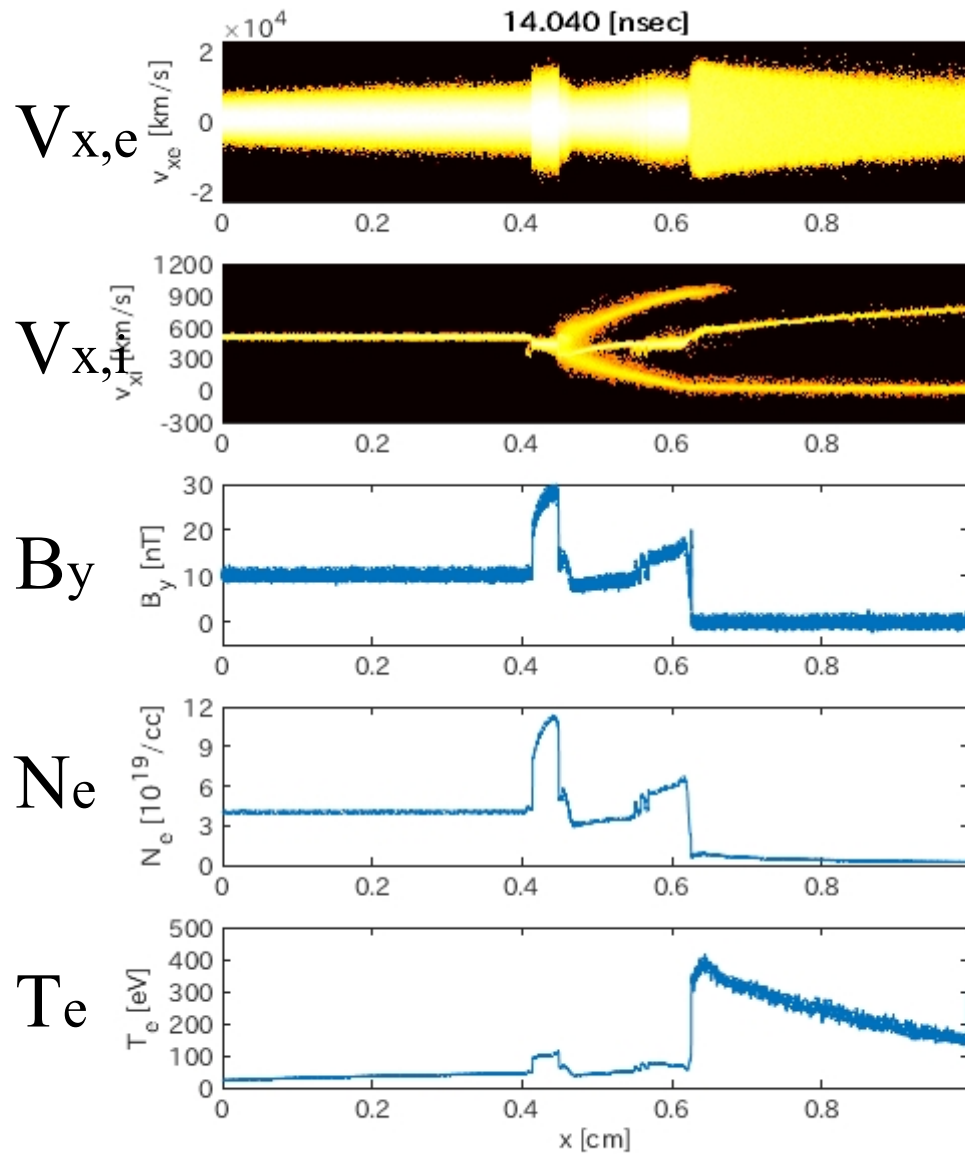
1次元(速度や電磁場はy,z成分を持つが、全ての物理量はx座標のみに依る。)

1D PIC simulations : Umeda, RY+ ('19)

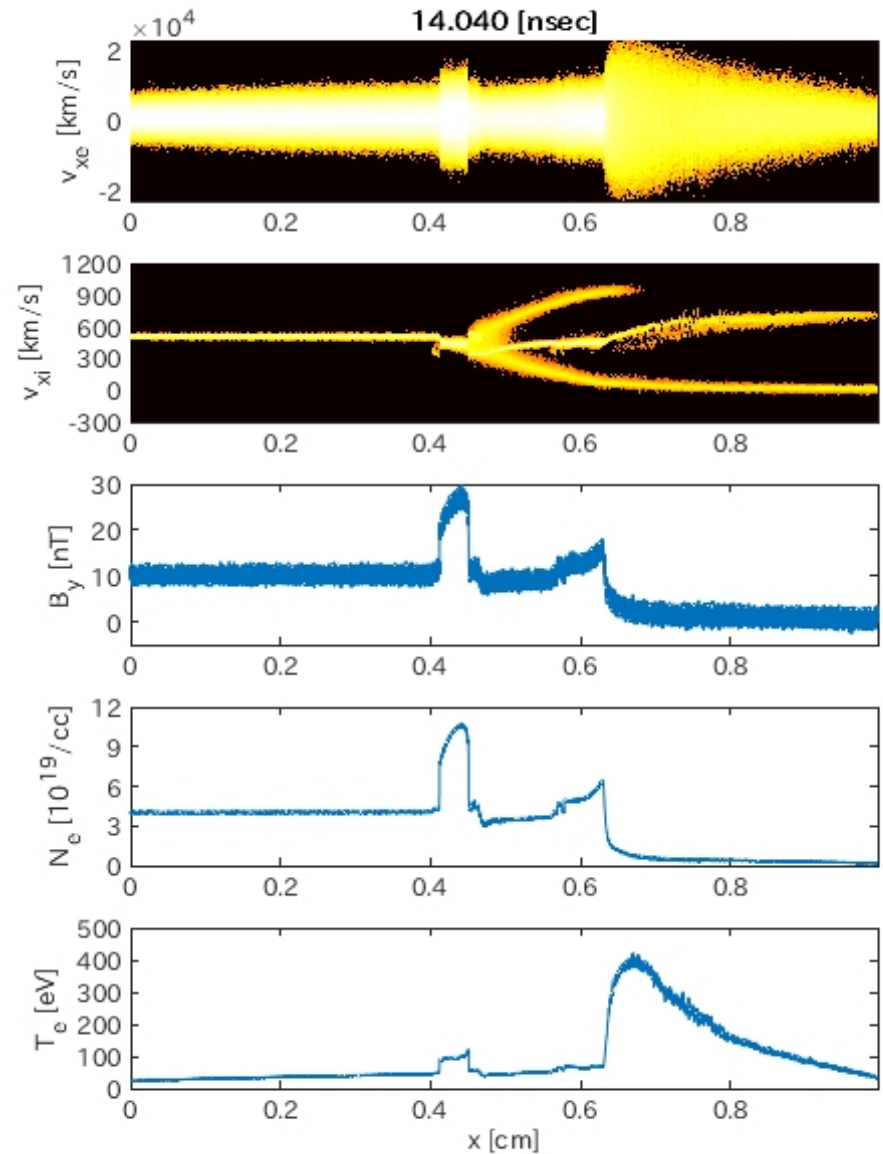
Quantity	Aluminum plasma	Nitrogen plasma
Drift velocity V_d [km/s]	500	0
Magnetic field B_0 [T]		
Run 1	10.0	0.5
Run 2	10.0	0.0
Run 3	0	0.5
Run 4	0	0.0
Electrons		
Density N_e [cm^{-3}]	3.75×10^{19}	1.5×10^{18}
Plasma frequency f_{pe} [Hz]	$5.51 \times 10^{13} / 5.51 \times 10^{12}$	$1.1 \times 10^{13} / 1.1 \times 10^{12}$
Temperature T_e [eV]	10	30
Thermal velocity V_{te} [km/s]	1,330	2,300
Debye length λ_{De} [m]	$3.71 \times 10^{-9} / 3.71 \times 10^{-8}$	$3.32 \times 10^{-8} / 3.32 \times 10^{-7}$
Inertial length d_e [m]	8.39×10^{-7}	4.33×10^{-6}
Cyclotron frequency f_{ce} [Hz]	2.8×10^{11}	1.4×10^{10}
Thermal gyro radius r_e [m]	7.55×10^{-7}	2.62×10^{-5}
Plasma beta	1.62	72.99
Ions		
Charge number Z	9	3
Mass ratio m_i/m_e	49572	25704
Density N_i [cm^{-3}]	4.17×10^{18}	5.0×10^{17}
Plasma frequency f_{pi} [Hz]	$7.43 \times 10^{11} / 7.43 \times 10^{10}$	$1.19 \times 10^{11} / 1.19 \times 10^{10}$
Temperature T_e [eV]	10	30
Thermal velocity V_{ti} [km/s]	5.97	14.3
Debye length λ_{Di} [m]	$3.71 \times 10^{-9} / 3.71 \times 10^{-8}$	$3.32 \times 10^{-8} / 3.32 \times 10^{-7}$
Inertial length d_i [m]	6.23×10^{-5}	4.01×10^{-4}
Cyclotron frequency f_{ci} [Hz]	5.08×10^7	1.63×10^6
Thermal gyro radius r_i [m]	1.87×10^{-5}	1.4×10^{-3}
Alfvén velocity V_A [km/s]	19.99	4.11
Plasma beta	0.18	24.33
Grid spacing Δx [m]		8.3×10^{-8}
Time step Δt [sec]		2.6×10^{-15}
Number of grids N_x		120,000
Number of steps N_t		6,000,000
Speed of light c [km/s]		$300,000 / 30,000$ (laboratory) / (numerical)

For magnetized Al piston plasma: $B(\text{Al}) = 10 \text{ T}$

Ambient: $B(\text{Nitrogen}) = 0$

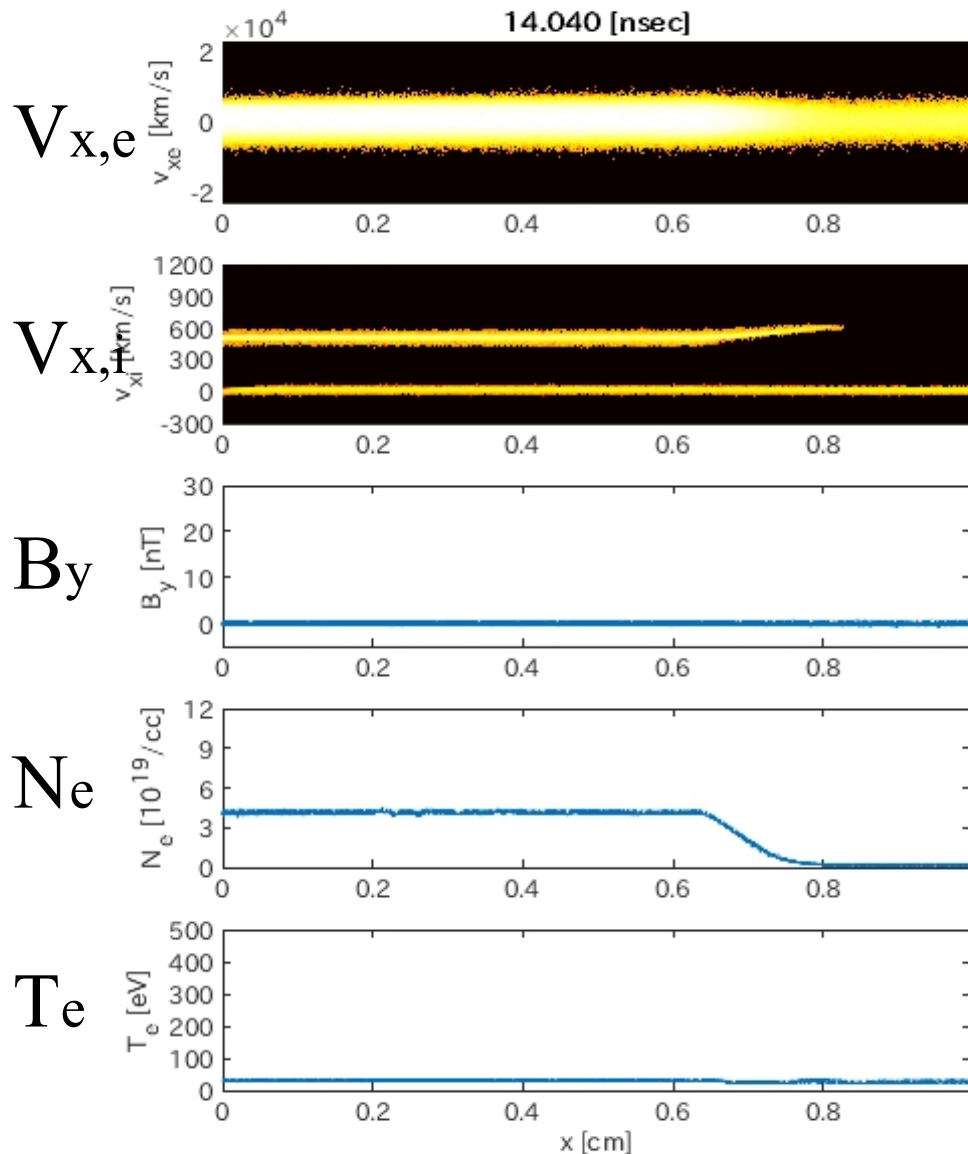


Ambient: $B(\text{Nitrogen}) = 0.5 \text{ T}$

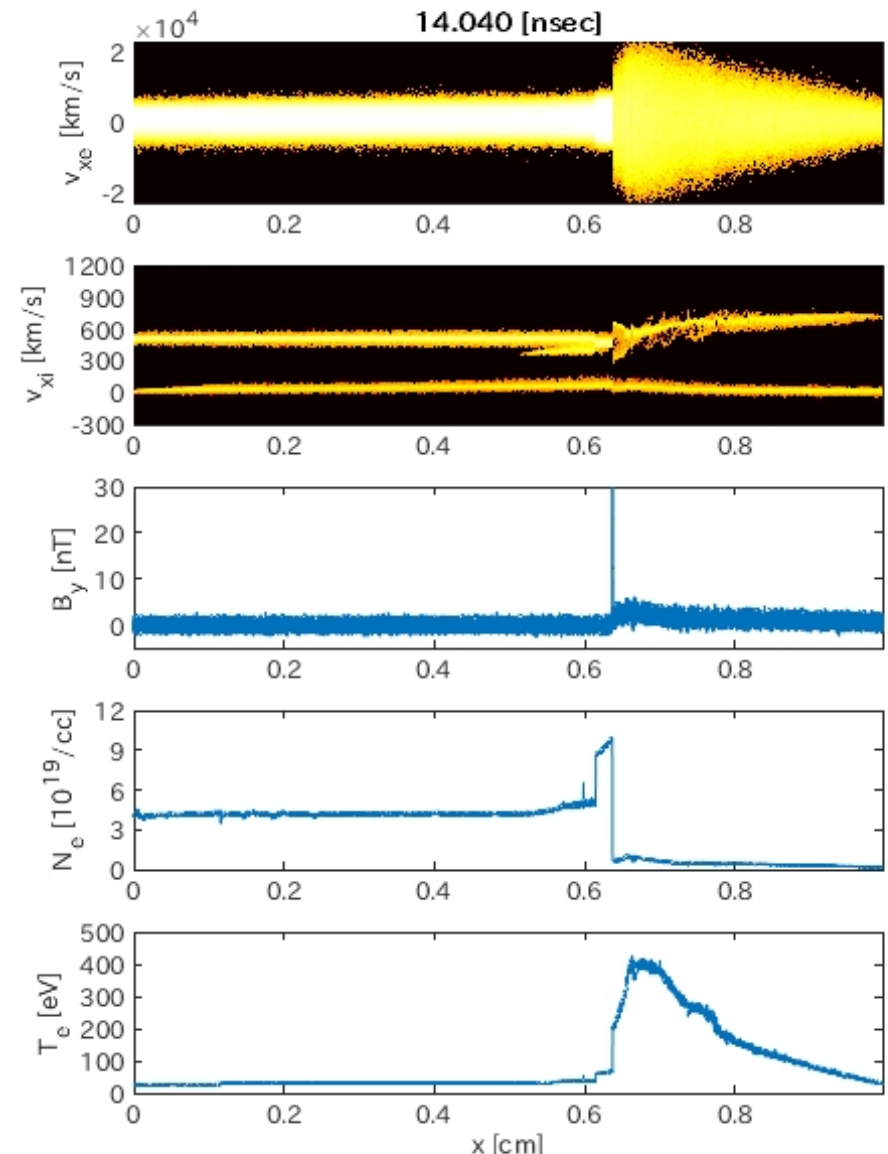


For un-magnetized Al piston plasma: $B(\text{Al}) = 0 \text{ T}$

Ambient: $B(\text{Nitrogen}) = 0$

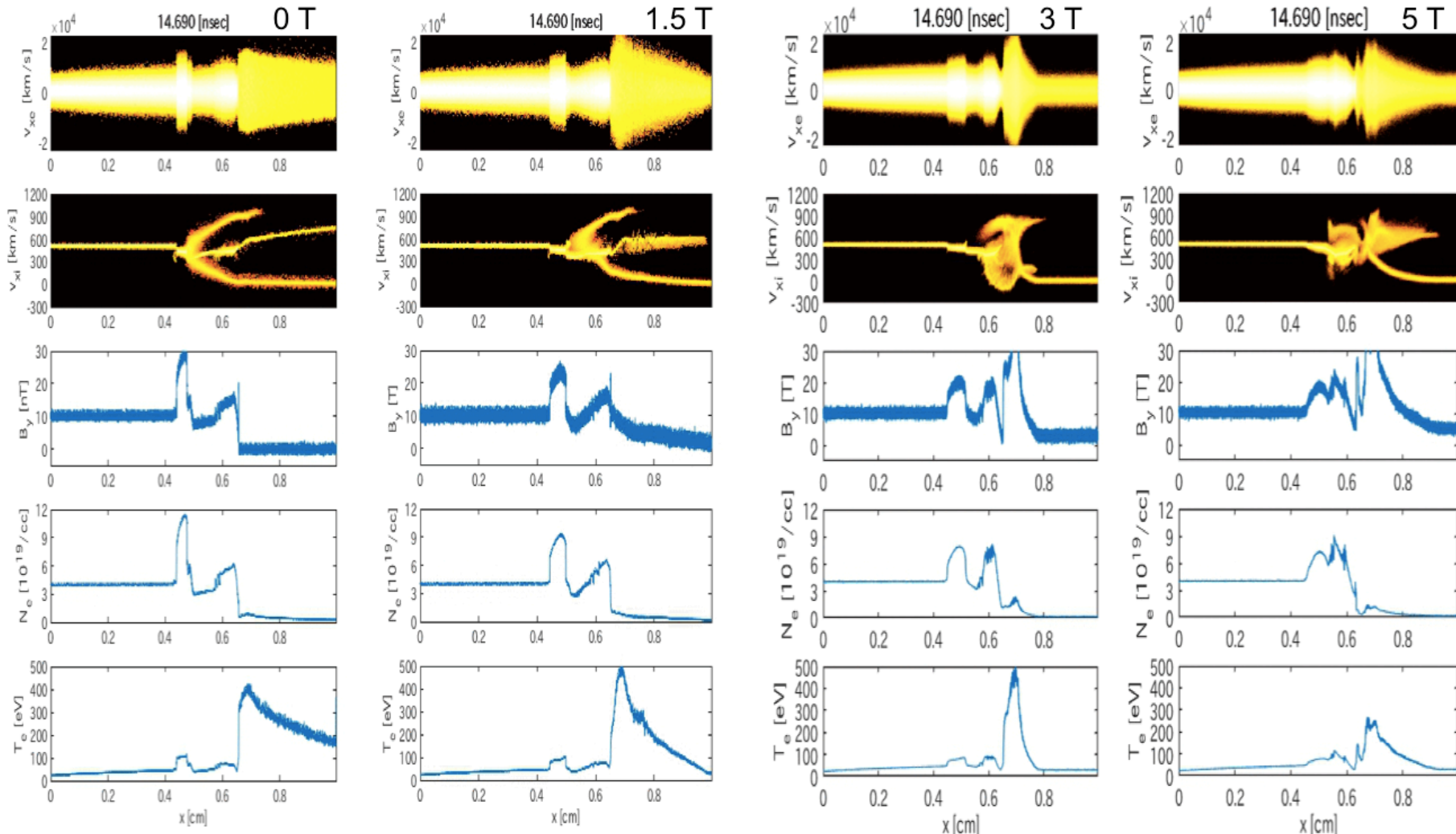


Ambient: $B(\text{Nitrogen}) = 0.5 \text{ T}$



1-dim PIC Simulations

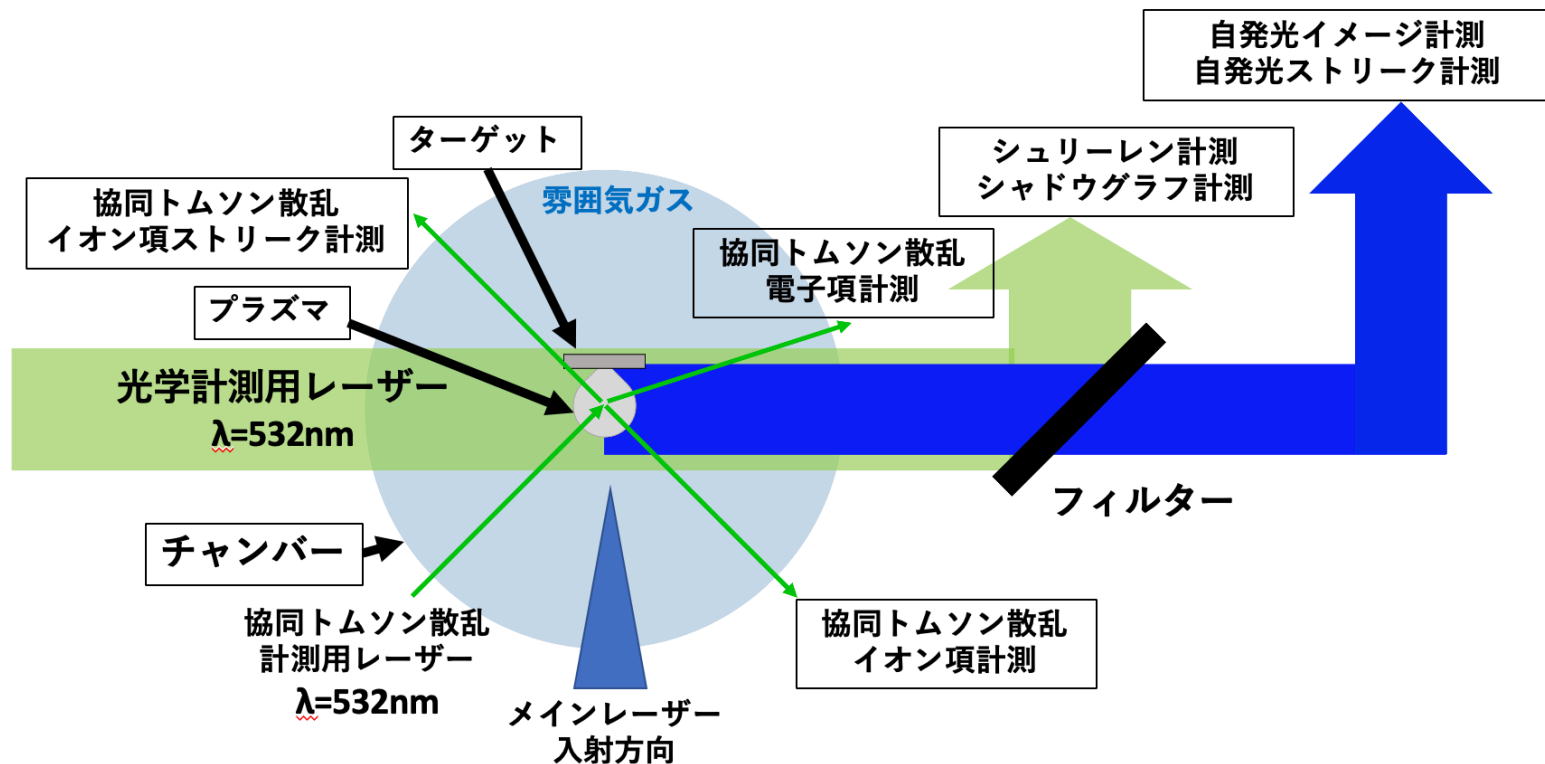
Al plasmas are injected at the left boundary into the Nitrogen plasmas initially at rest.
Behavior of the driven Nitrogen plasmas depend on ambient perpendicular magnetic field.



(see Umeda et al. 2019, Phys. Plasmas)

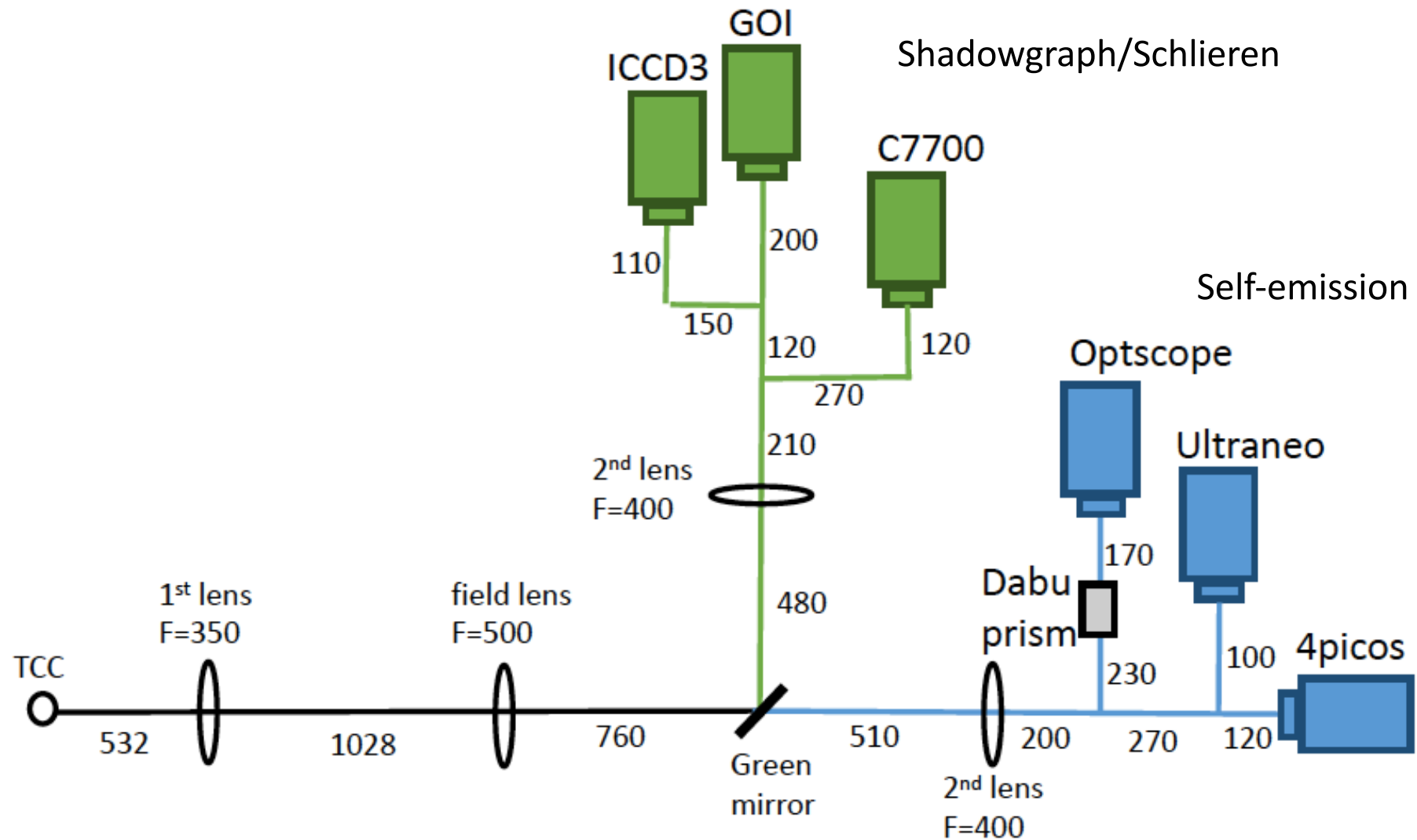
Diagnostics

- Self emission (optical; brems & lines): from high-T regions.
- Shadowgraph: tracing 2nd derivative of n_e.
- Interferometry: tracing n_e
- Collective Thomson scattering: T_e, T_i, n_e, Z, bulk flow velocity
- B-field measurements: B-dot w/ coil, proton backlight

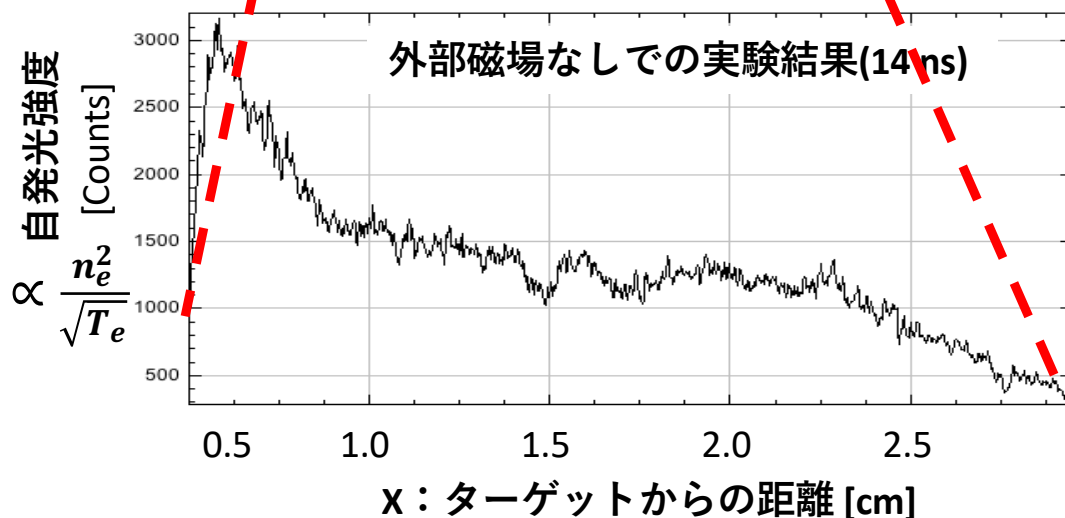
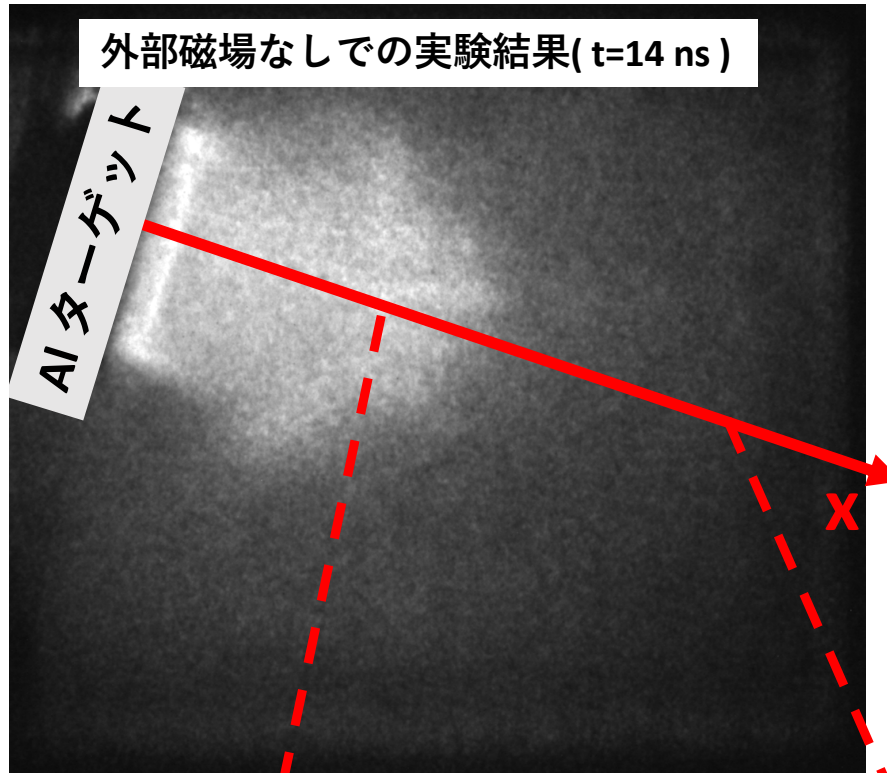


Diagnostics

2017～2019年度の光学計測系



自発光強度分布(窒素側の外部磁場なし)



実験での自発光計測 $\propto \frac{n_e^2}{\sqrt{T_e}}$ において、窒素の磁場が無い場合でも、AI プラズマと窒素プラズマの相互作用が確認された。

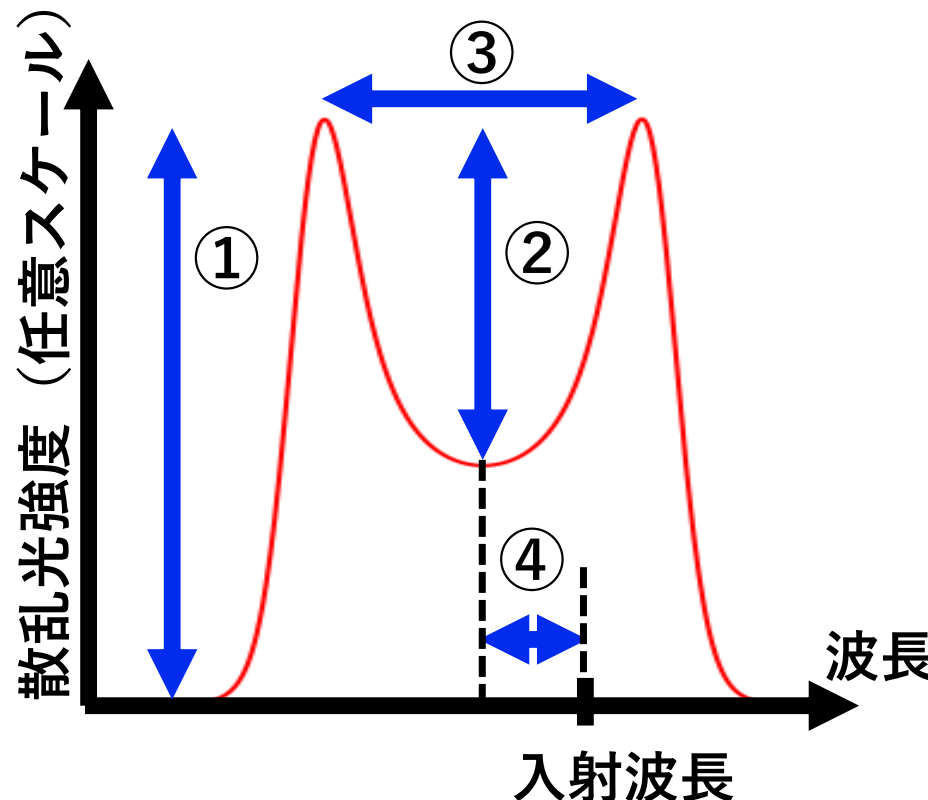
→AI プラズマは自己生成磁場で磁化されていると考えられる。

粒子シミュレーションの結果とも、定性的に N_e, T_e の振る舞いが一致。
(詳細は石坂講演)

トムソン散乱計測

プラズマの集団運動が顕著な場合のトムソン散乱のスペクトル形状は2つのピークを持つ。

プラズマ中に励起されるイオン音波
(ほぼflowの方向に伝播) と入射単色光
との共鳴相互作用。
2つのピークはその共鳴に対応。



モデルパラメータ：

1. 電子密度
2. 電子温度
3. イオン温度
4. イオンの平均価数
5. flow速度

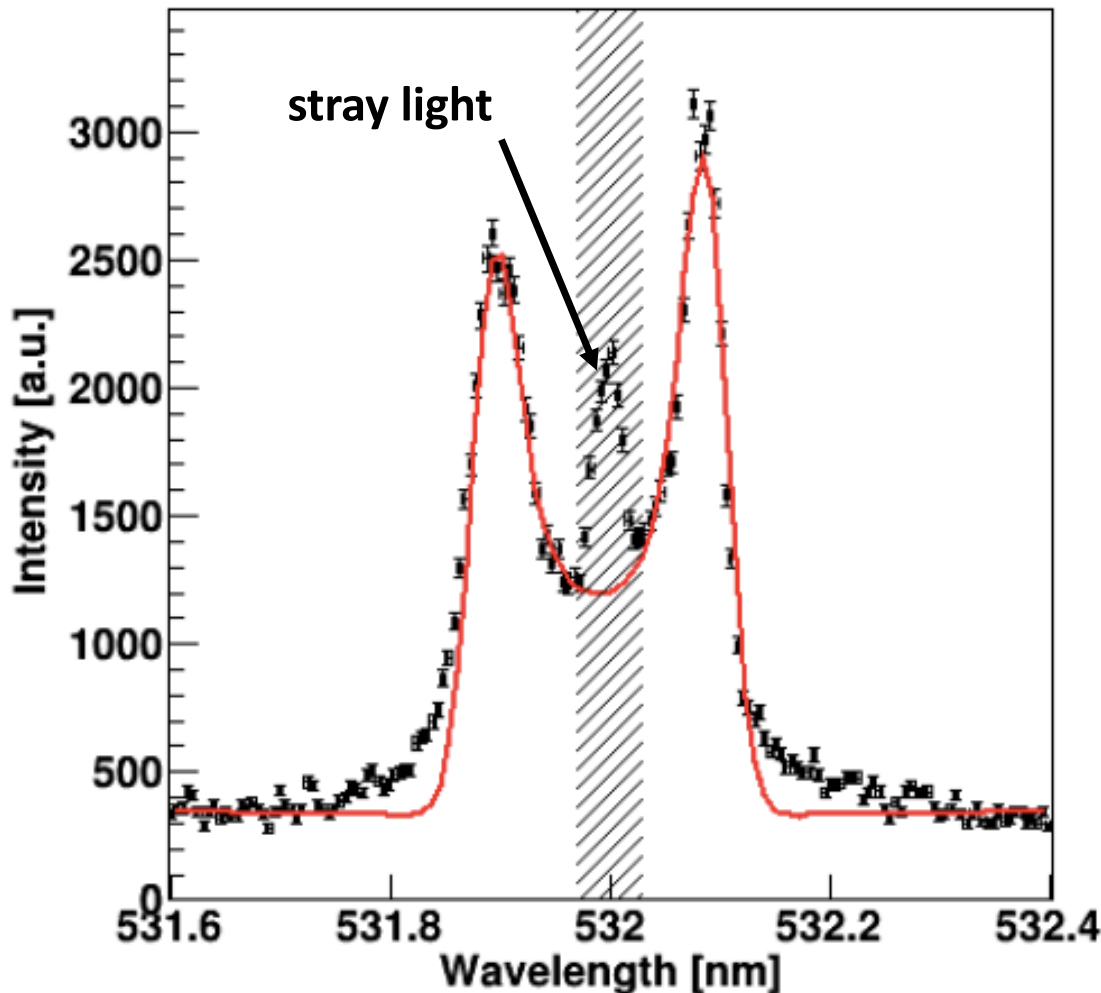
スペクトルから決定できる量

1. 散乱光強度
2. ピークとボトムの強度比
3. ピーク間距離
4. 入射波長と中心波長のずれ

仮定を1つ追加すれば、
フィッティングにより5つのパラメータを決定できる。

Example of TS fitting

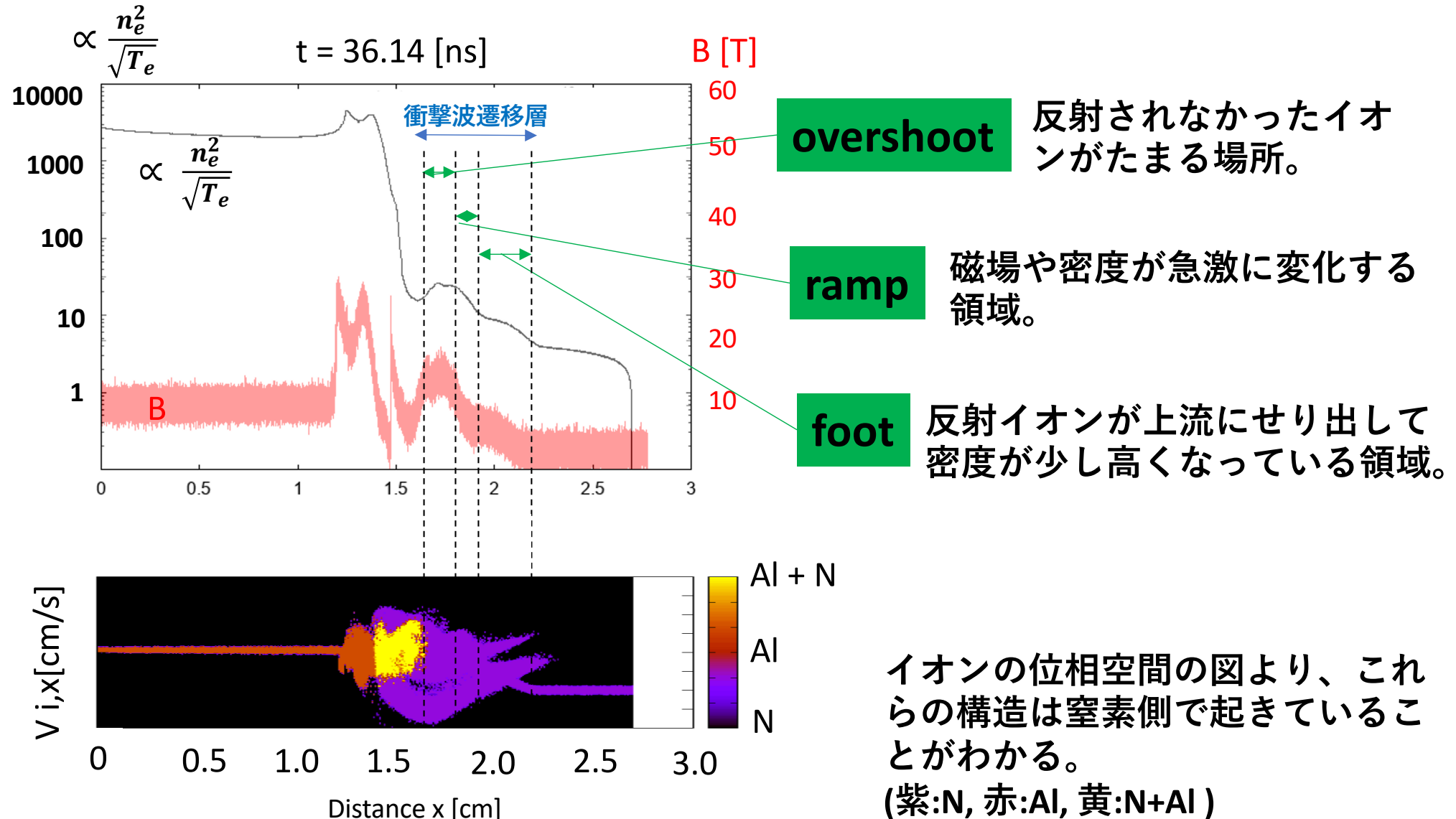
Thomson scattering (TS) spectrum
at TCC (=1.4 cm from target), 17 ns after shot.



Derived parameters:
 $n_e = 1.0 \times 10^{18} \text{ cm}^{-3}$
 $T_e = 94 \text{ eV}$
 $T_i = 30 \text{ eV}$
 $Z = 3.2$
 $v_e - v_i = 150 \text{ km/s},$
where we assumed
N-gas (5torr) is fully ioniz

無衝突衝撃波の生成(pic simulation)

外部磁場を 3T印加した粒子シミュレーションでは、衝撃波内部で反射されたイオンの影響を反映した衝撃波の構造が確認できた。



Summary

- **No external magnetic field case:**

Density jump, which is detected by SOP, is not the shock front but the electron MHD tangential discontinuity.

- **External magnetic field cases ($B = 3.6 \text{ T}$):**

- * We detected forming collisionless shocks with $M_A \sim 10$ that propagates into magnetized plasma.

New experiments with $B \sim 3\text{T}$ will start in the next October!

Measure the temperature anisotropy!